

**Distribution Agreement**

In presenting this thesis as a partial fulfillment of the requirements for a degree from Emory University, I hereby grant to Emory University and its agents the non-exclusive license to archive, make accessible, and display my thesis in whole or in part in all forms of media, now or hereafter now, including display on the World Wide Web. I understand that I may select some access restrictions as part of the online submission of this thesis. I retain all ownership rights to the copyright of the thesis. I also retain the right to use in future works (such as articles or books) all or part of this thesis.

Yike Teresa Shi

April 2, 2024

Transmission Bottleneck Size Estimation from De Novo Viral Genetic Variation

by

Yike Teresa Shi

Katia Koelle  
Adviser

Department of Biology

Katia Koelle  
Adviser

Rustom Antia  
Committee Member

Max Lau  
Committee Member

2024

Transmission Bottleneck Size Estimation from De Novo Viral Genetic Variation

By

Yike Teresa Shi

Katia Koelle  
Adviser

An abstract of  
a thesis submitted to the Faculty of Emory College of Arts and Sciences  
of Emory University in partial fulfillment  
of the requirements of the degree of  
Bachelor of Science with Honors

Department of Biology

2024

## Abstract

### Transmission Bottleneck Size Estimation from De Novo Viral Genetic Variation

By Yike Teresa Shi

Sequencing of viral infections has become increasingly common over the last decade. Deep sequencing data in particular have proven useful in characterizing the roles that genetic drift and natural selection play in shaping within-host viral populations. They have also been used to estimate transmission bottleneck sizes from identified donor–recipient pairs. These bottleneck sizes quantify the number of viral particles that establish genetic lineages in the recipient host and are important to estimate due to their impact on viral evolution. Current approaches for estimating bottleneck sizes exclusively consider the subset of viral sites that are observed as polymorphic in the donor individual. However, these approaches have the potential to substantially underestimate true transmission bottleneck sizes. Here, we present a new statistical approach for instead estimating bottleneck sizes using patterns of viral genetic variation that arise de novo within a recipient individual. Specifically, our approach makes use of the number of clonal viral variants observed in a transmission pair, defined as the number of viral sites that are monomorphic in both the donor and the recipient but carry different alleles. We first test our approach on a simulated dataset and then apply it to both influenza A virus sequence data and SARS-CoV-2 sequence data from identified transmission pairs. Our results confirm the existence of extremely tight transmission bottlenecks for these 2 respiratory viruses.

Transmission Bottleneck Size Estimation from De Novo Viral Genetic Variation

By

Yike Teresa Shi

Katia Koelle  
Adviser

A thesis submitted to the Faculty of Emory College of Arts and Sciences  
of Emory University in partial fulfillment  
of the requirements of the degree of  
Bachelor of Science with Honors

Department of Biology

2024

## Acknowledgements

I would like to express my deepest gratitude to Dr. Katia Koelle for unwavering support and guidance throughout the project. Her knowledge, discernment, and commitment have been crucial in forming this project and advancing my career as a researcher. I also could not have undertaken this journey without my honors committee, Rustom Antia and Max Lau, who generously provided valuable feedback and helped to polish the research project. I would like to extend my sincere thanks to my family, friends, and lab members who have shared my joys and worries and have been supporting me all the time. Lastly, I would like to thank my kitten Mochi for all the entertainment and emotional support.

Table of Contents

**Introduction..... 1**

**Methods ..... 4**

    The Stochastic Within-Host Model .....4

    Derivation of the Probability Distribution for the Number of Clonal Variants.....8

**Results..... 10**

    Application to Simulated Data.....10

    Application to Empirical Data .....15

    Application to IAV .....16

    Application to SARS-CoV-2 .....19

    Guarding Against the Erroneous Calling of Clonal Variants .....21

    Considering Alternative Distributions for the Initial Number of Viral Particles That Start an Infection24

**Discussion..... 27**

**Supplemental Material..... 31**

    Derivation of the probability distribution for the number of clonal variants.....31

    Rederivation of the Bozic et al. (2016) equation for the mean number of clonal variants.....38

    Calculation of the mean transmission bottleneck size **N<sub>b</sub>**.....39

    Quantification of the number of clonal variants for the influenza A virus data set.....39

    Quantification of the number of clonal variants for the SARS-CoV-2 data set .....40

    Probability of a donor iSNV transmitting and fixing in a recipient.....41

**Supplemental Tables ..... 42**

**Supplemental Figures ..... 43**

**References ..... 51**

## Introduction

In viral infections, transmission bottleneck sizes are defined as the number of viral particles transmitted from a donor to a recipient host that successfully establish genetic lineages within the recipient. Quantifying the magnitude of these bottlenecks is important for understanding the ecological and evolutionary dynamics of viruses at multiple scales, as these bottlenecks bridge processes occurring at within-host and between-host levels (Zwart and Elena 2015; McCrone and Lauring 2018). At the level of the population, tight transmission bottlenecks can act to slow down the rate of viral adaptation, as beneficial mutations that arise within a donor host can be lost during transmission to a recipient host (Abel et al. 2015; Zaraket et al. 2015; Zwart and Elena 2015; Geoghegan et al. 2016). However, they may also be advantageous to a viral population, for example by enabling its path through a rugged fitness landscape and by purging cheaters from its population (Zwart and Elena 2015). At the within-host level, tight transmission bottlenecks lead to lower levels of viral genetic diversity in recipient hosts and genetic drift playing an important role in shaping the viral population during the early stages of a recipient's infection (Gutiérrez et al. 2012; Abel et al. 2015; Zwart and Elena 2015; McCrone and Lauring 2018; McCrone et al. 2018). Finally, quantifying transmission bottleneck sizes is important for more applied reasons: having estimates of the bottleneck size may help determine whether it is possible to reconstruct who-infected-whom in an outbreak setting and will determine which inference methods might be the most suitable to use in a specific application (Hall et al. 2016; Campbell et al. 2018; Duault et al. 2022).

Several statistical methods have recently been developed to estimate transmission bottleneck sizes from viral deep-sequencing data (Emmett et al. 2015; Zwart and Elena 2015; Sobel Leonard et al. 2017b; Ghafari et al. 2020). All of these approaches rely on patterns of



shared genetic variation by first characterizing the genetic variation that is present in both the donor and the recipient of an identified transmission pair. They then restrict their analyses to the subset of sites that are polymorphic in the donor. One approach (the presence/absence method) estimates bottleneck sizes by asking which of the variants identified in the donor are also detected in the recipient and which are not. A second approach (the binomial sampling method) instead makes use of variant frequencies quantified in the recipient, rather than just their presence or absence. However, it assumes that the observed differences in variant frequencies between a donor and a recipient arise from the process of viral sampling alone (Emmett et al. 2015; Poon et al. 2016). A third approach (the betabinomial sampling method) similarly makes use of variant frequencies from the recipient but additionally accounts for deviations between donor and recipient variant frequencies that arise from demographic noise during the early period of exponential viral growth in the recipient (Sobel Leonard et al. 2017b). Finally, a haplotype-based approach to transmission bottleneck size estimation has been developed (Ghafari et al. 2020); it extends the betabinomial sampling method to account for genetic linkage between loci.

Applications of these inference methods to viral sequence data have indicated that transmission bottlenecks are tight for many viral pathogens. Several studies have estimated bottleneck sizes of 1–3 viral particles for plant viruses (Moury et al. 2007; Betancourt et al. 2008; Sacristán et al. 2011). Tight transmission bottlenecks of 1–5 viral particles have also been estimated for human viruses, including influenza viruses (McCrone et al. 2018; Valesano et al. 2020), HIV-1 (Keele et al. 2008), and most recently SARS-CoV-2 (Braun et al. 2021a, 2021b; Lythgoe et al. 2021; Martin and Koelle 2021; Nicholson et al. 2021; Wang et al. 2021; Li et al. 2022; Bendall et al. 2023). When bottlenecks are tight, as in these cases, there is little genetic diversity that is transferred from a donor to a recipient. For acute infections, with little time to

accrue new mutations, this often times leads to overall low levels of viral diversity in infected hosts. When there is no viral genetic diversity observed in a donor sample, estimation of transmission bottleneck size is not possible for that transmission pair. Studies that estimate bottleneck sizes (such as the ones cited above) therefore often rely on combining data from across a large number of transmission pairs to quantify an average bottleneck size. Within experimental settings, barcoded viruses can be used to increase host genetic diversity and thereby to improve resolution of transmission bottleneck sizes (Varble et al. 2014; Amato et al. 2022). However, natural settings do not afford us with this possibility.

Three issues need to be considered when interpreting bottleneck size estimates derived from inference methods that rely on patterns of shared genetic variation. One issue is that the time of the infectious contact is not known in many cases, and the donor is unlikely to be sampled exactly at the point of transmission. Longitudinal studies of acute infections have indicated that variant frequencies can change rapidly over the course of infection, with many variants that are observed on one day not being observed on an adjacent day (McCrone et al. 2018; Popa et al. 2020; Valesano et al. 2020). These rapid variant frequency changes in the donor will act to considerably depress inferred bottleneck size estimates, as the assumed allele frequencies at the time of transmission will deviate from the true ones. A second issue is that rapid variant frequency changes in the recipient will similarly act to depress inferred bottleneck size estimates, as transmitted genetic variation could be lost in the recipient even when viral titers are high. The extent of shared genetic variation between a donor and a recipient may therefore be more indicative of the extent of viral genetic drift within individual infections than the size of the transmission bottleneck. A third issue is that existing methods all assume that viral particles that initiate infection in the recipient are randomly sampled from the donor. However, it

could be the case that genetically similar virions are aggregated and transmit together, as would be the case with collective infectious units (Sanjuán 2017). If this is the case, one would again erroneously infer bottleneck sizes to be tight when they might in fact be loose.

Here, we develop an approach for estimating transmission bottleneck sizes that instead makes use of de novo genetic variation that is observed in a recipient. Similar to some existing approaches, it assumes that all observed genetic variation is neutral and that the viral population in the recipient host undergoes stochastic exponential growth. It differs from existing approaches, however, in that it uses a different subset of sites for inference, namely sites that are monomorphic in both the donor and recipient but carry different alleles. Consideration of these sites, rather than sites that are polymorphic in the donor, circumvents the 3 issues described above. To introduce our approach, we first describe the stochastic model that we assume underlies the process of viral population expansion in a recipient. We then describe the inference framework and test our approach on simulated data, showing that it accurately recovers transmission bottleneck sizes. Finally, we apply our approach to data from influenza A virus (IAV) and SARS-CoV-2 transmission pairs, confirming previous findings of tight transmission bottlenecks for these respiratory viruses using an approach that is not prone to underestimating this quantity.

## **Methods**

### ***The Stochastic Within-Host Model***

We model the dynamics of the viral population within a recipient using a multitype branching process model. The types in this model correspond to different viral genotypes. Because we assume that all mutations are neutral, each type has the same overall offspring

distribution. More specifically, we assume a geometric offspring distribution, consistent with the offspring distribution under a stochastic birth–death model. The geometric distribution is parameterized with a success probability of  $p_{geom}$ , where  $p_{geom} = 1/(R_0 + 1)$  and  $R_0$  is the within-host basic reproduction number. As such, the expected number of offspring a given viral particle leaves is given by  $R_0$ . The number of mutations that occur during the production of a viral offspring is assumed to be Poisson-distributed with mean  $\mu$ . When one or more mutations occur during the production of an offspring, the resultant offspring becomes a new type. As such, we assume infinite sites. In addition to carrying any new mutations, offspring inherit the mutations of their parent. Because we model the virus population as asexually reproducing, genetic linkage across the virus genome is assumed to be complete. Because we are interested in characterizing transmission dynamics between infections, we consider only the supercritical case corresponding to a within-host basic reproduction number of  $R_0 > 1$ .

The virus population starts with an initial population size of  $N$  viral particles, which stem from the donor’s virus population.  $N$  is related, but not equivalent, to the transmission bottleneck size  $N_b$ . This is because  $N_b$  quantifies the number of viral particles that succeed in establishing a genetic lineage in the recipient and some of the  $N$  initial viral particles may have lineages that do not successfully establish but instead go stochastically extinct. As such  $N_b \leq N$ . All  $N$  initial viral particles harbor 0 de novo mutations, where we define de novo mutations as mutations that occurred during viral replication in the recipient. These  $N$  initial viral particles could in principle be genetically distinct from one another. Any genetic variation that is present in these particles stems from the donor. Hereafter, we refer to viral particles without de novo mutations (including these  $N$  initial viral particles) as wild-type particles, while remaining cognizant that these could differ from one another genetically. We further define a wild-type lineage as a genetic lineage

that starts from an initial wild-type particle and includes the subset of offspring that are wild-type. Finally, we define a mutant lineage as a lineage that starts from a viral particle that is an immediate descendant of a wild-type particle and carries one or more mutations relative to that wild-type parent.

We can lay out all of the possible dynamic outcomes of this branching process model. The first possible outcome is that the virus population in the recipient goes stochastically extinct (Fig. 1A). This would result in the recipient remaining uninfected and (necessarily, but trivially) 0 mutant lineages successfully establishing in the recipient. The second possible outcome is that at least one of the  $N$  initial viral particles seeds a wild-type lineage that successfully establishes (Fig. 1B). In this case, there will theoretically be an infinite number of mutant lineages that will successfully establish. This is because under a supercritical branching process the wild-type viral population will ultimately grow geometrically at a per generation rate of  $R_0 e^{-\mu}$ , and each of the wild-type viral particles in this ever-growing population may give rise to a mutant lineage that will also establish in the viral population. In reality, viral population sizes will expand and then decline in an acute infection, such that there will be many, but not an infinite number of mutant viral lineages that establish initially, only to die out toward later stages of an infection. The third possible outcome is that no wild-type viral lineages establish but a single mutant lineage, seeded by a wild-type viral particle, establishes (Fig. 1C). Finally, the fourth possible outcome is that no wild-type viral lineages establish but 2 or more mutant lineages establish (Fig. 1D). In the case of a successful infection (Fig. 1B–D), the overall viral population will grow geometrically at rate  $R_0$  once the population has reached a large size. Again, in reality, viral population sizes in an acute infection will increase and then decrease. Successful sequencing of a viral sample from a recipient, however, will occur when viral titers are still relatively high.

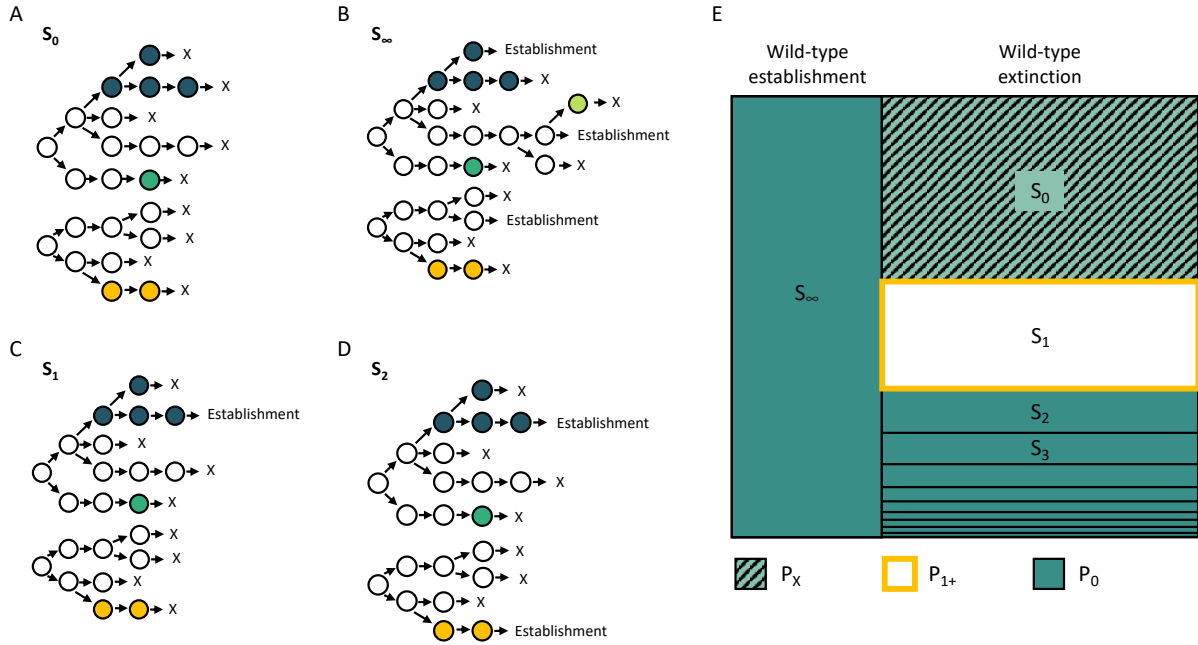


**Fig. 1. Possible dynamic outcomes in the recipient.** **A)** The viral population in the recipient may go stochastically extinct, leading to no infection in the recipient. **B)** One or more wild-type lineages may successfully establish. **C)** No wild-type lineages establish but a single mutant lineage successfully establishes. **D)** No wild-type lineages establish but 2 or more mutant lineages successfully establish. Here, we show a scenario of 2 mutant lineages successfully establishing. Outcomes (B–D) result in successful infection of the recipient. Wild-type particles are shown in white. Mutant lineages are shown in different colors. In (A–D),  $N = 2$  initial viral particles and  $S_l$  denotes the number of mutant lineages  $l$  that successfully establish under each scenario. **E)** Summary of possible dynamic outcomes, with  $S_l$  again denoting the number of mutant lineages  $l$  that establish. Outcomes are color-coded by the number of clonal variants  $k$  that would be observed under the outcome. The portion of the outcome space labeled  $P_X$  denotes the probability that the viral population in the recipient goes extinct. The portion of the outcome space labeled  $P_0$  denotes the probability that  $k = 0$  clonal variants establish in the recipient’s viral population. The portion of the outcome space labeled  $P_{1+}$  denotes the probability that at least 1 clonal variant establishes in the recipient’s viral population.

For a given outcome, we can quantify the number of variants that arose and fixed in the viral population of the recipient. We refer to these variants as clonal variants. In the case of the viral population going extinct (the first outcome; Fig. 1A), the infection in the recipient did not establish and we will not have observed this outcome in a transmission pair. We refer to the probability of this outcome as  $P_X$ . In the case of one or more of the wild-type viral lineages establishing (the second outcome; Fig. 1B), the number of clonal variants will be 0, because none

of the mutations that arose in any of the mutant lineages will fix. In the case of no wild-type viral lineages establishing but 2 or more mutant lineages successfully establishing (the fourth outcome; Fig. 1D), the number of clonal variants will similarly be 0, because none of the mutations that arose in any of the mutant lineages will fix under an infinite sites assumption. Finally, in the case of no wild-type viral lineages establishing but exactly one mutant lineage successfully establishing (the third outcome; Fig. 1C), the number of clonal variants will be at least one. It will be exactly one if only a single mutation occurred during the generation of the mutant lineage and no additional clonal variants arose in this mutant lineage. It will be greater than one if more than one mutation occurred during the generation of the mutant lineage and/or additional mutations occurred in this mutant lineage that ultimately fixed. Figure 1E graphically summarizes all of these possible dynamic outcomes.

### ***Derivation of the Probability Distribution for the Number of Clonal Variants***

The multitype branching process model, resulting in the different possible outcomes shown in Fig. 1, contains 3 parameters: the initial wild-type viral population size  $N$ , the within-host basic reproduction number  $R_0$ , and the per genome, per infection cycle mutation rate  $\mu$ . Here, we are specifically interested in estimating the initial viral population size  $N$ . Estimates of  $N$  will be used to calculate the transmission bottleneck size  $N_b$ . To estimate  $N$ , we need to ask: for a given recipient harboring  $k$  clonal variants, what is the likelihood that the initial viral population size was  $N = 1, 2, 3, \dots$ ? These likelihoods can be calculated if we can calculate the probability distribution for a recipient harboring  $k = 0, 1, 2, \dots$  clonal variants, for given values of  $N$ ,  $R_0$ , and  $\mu$ . In the Supplementary Material, we derive the expression for this probability distribution based on the different possible dynamic outcomes shown in Fig. 1E, with associated supplementary fig. S1 graphically depicting the steps involved in this derivation.

We can confirm the accuracy of our analytical results in 2 ways. First, previous work by Bozic et al. (2016), in the context of cancer cell dynamics, derived an equation for the number of clonal variants one would expect in a population undergoing birth–death dynamics, given an initial population size of  $N = 1$ . This expected number is given by  $\delta u / (1 - \delta)$ , where their parameter  $\delta$  corresponds to  $1/R_0$  and their mutation parameter  $u$  corresponds to our  $\mu$ , under the assumption that  $\mu$  is small ( $\ll 1$ ). Figure 2A shows the expected number of clonal variants across a range of within-host  $R_0$  and across a range of mutation rates  $\mu$ , as calculated from their equation. In Fig. 2B, we plot the expected number of clonal variants as given by our analytical results under the assumption of  $N = 1$ . The quantitative similarity of the plots shown in Fig. 2A and b demonstrates the accuracy of our clonal variant derivation. In the Supplementary Material, we further show how we can derive their equation using our analytical expressions, under the assumption of a low mutation rate.

The second way we can check our analytical results is through extensive numerical simulation of the branching process model. For a given simulation, we can determine whether the viral population went stochastically extinct or whether infection was successful. For those simulations establishing successful infection, we can determine the number of clonal variants that evolved. To check our clonal variant derivation, we plot in Fig. 2C the fraction of simulations that resulted in  $k = 0, 1, 2, \dots$  clonal variants from 4,000 simulations that were each parameterized with an initial viral population size of  $N = 2$ , a within-host basic reproduction number of  $R_0 = 1.2$ , and a per genome per infection cycle mutation rate of  $\mu = 0.2$ . Alongside this empirical distribution, we plot the analytically derived clonal variant probabilities under this parameterization. The quantitative similarity of these distributions demonstrates the accuracy of our analytical derivations.



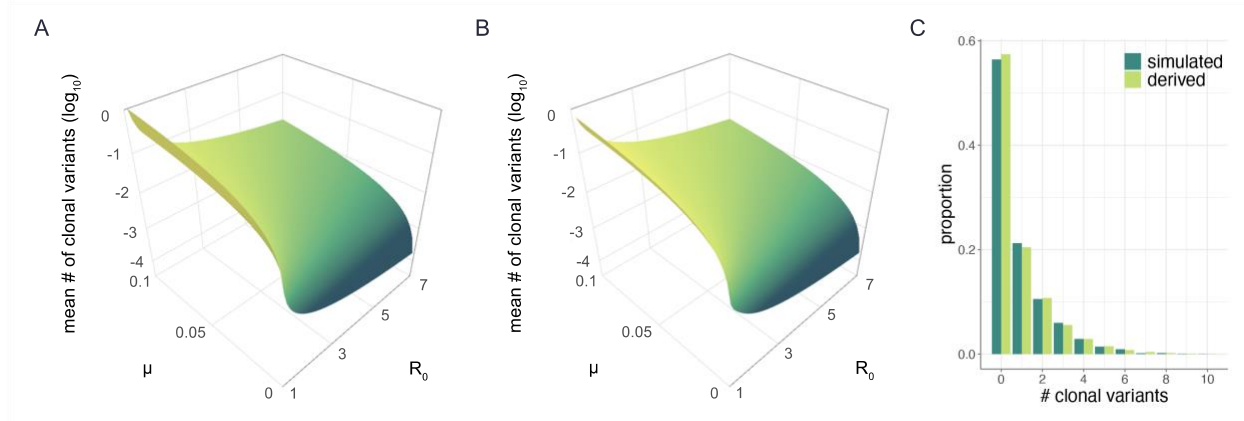


**Fig. 2. Confirmation of our analytical results.** **A)** The expected number of clonal mutations when  $N = 1$ , as derived by Bozic et al. (2016) using a birth–death model. Mean numbers of clonal mutations are shown across a range of within-host  $R_0$  and  $\mu$  parameter values. **B)** The mean number of clonal mutations, as calculated from our analytical expressions, parameterized with  $N = 1$ . **C)** Histogram showing the proportion of simulations that resulted in  $k = 0, 1, 2, \dots$  clonal variants (dark green), alongside our analytical predictions (light green). Simulated proportions were calculated using 4,000 stochastic simulations that resulted in successful infection. Simulations and analytical results shown in panel C were parameterized with  $N = 2$ ,  $R_0 = 1.2$ , and  $\mu = 0.2$ .

## Results

### *Application to Simulated Data*

Before applying our statistical method to sequence data from empirical transmission pair studies, we first applied our approach to simulated (mock) data. To this end, we forward simulated the branching process model until we obtained 100 successful recipient infections. Forward simulations were all performed with a within-host basic reproduction number of  $R_0 = 1/6$  and a per genome, per infection cycle mutation rate of  $\mu = 0.4$ . Instead of assuming that the initial viral population size  $N$  was the same across all recipients, we assumed that the initial number of viral particles was Poisson-distributed with mean  $\lambda = 2.1$  (Fig. 3A). (Simulations with a higher  $N$  had a lower chance of going stochastically extinct so higher  $N$  simulations were overrepresented in the mock dataset, which we account for, as described in greater detail below.)

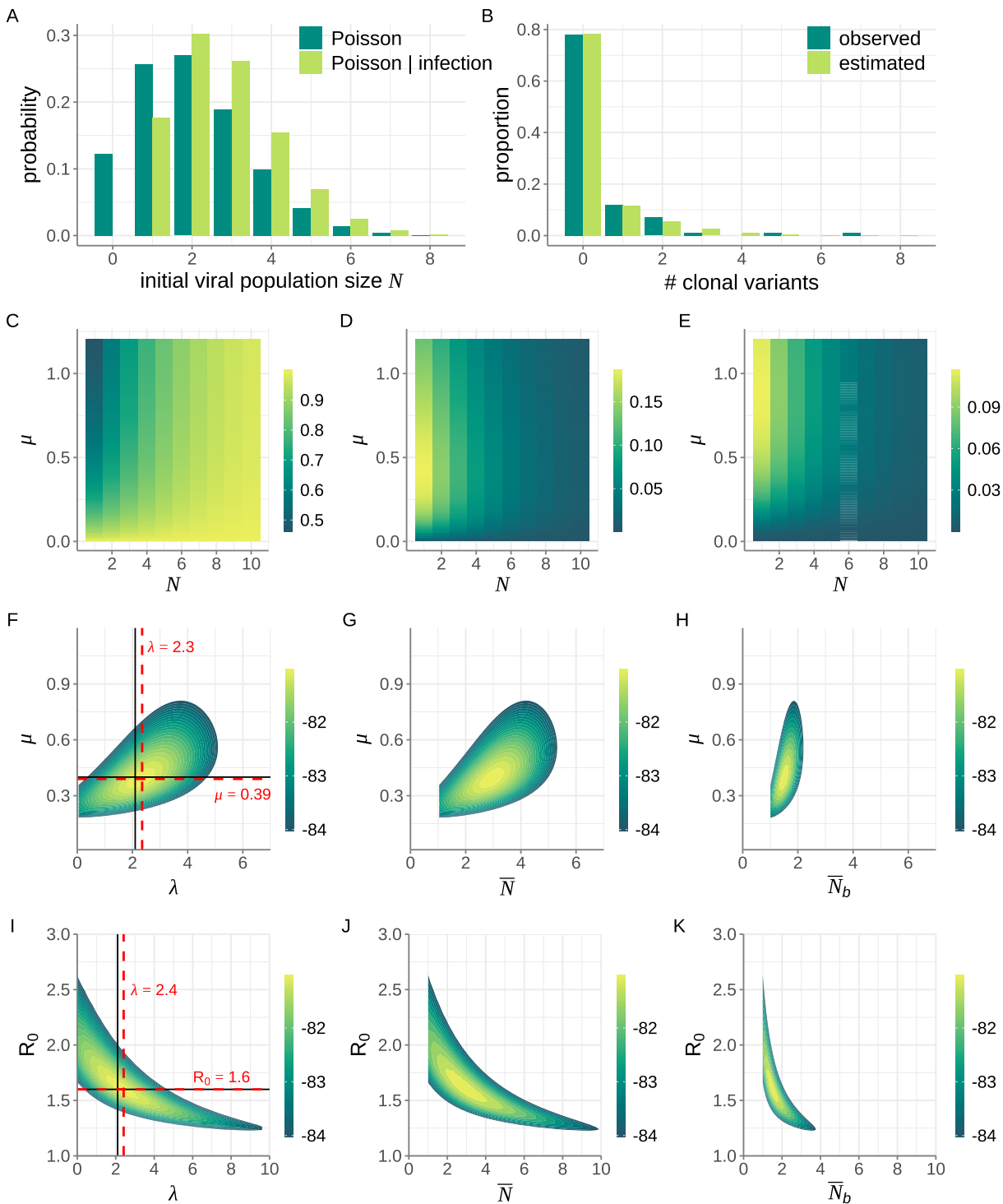


**Fig. 3. Application of our inference method to a mock dataset of 100 transmission pairs.** **A)** Poisson probability distribution showing the distribution of initial viral population sizes  $N$  that seed potential recipient infections (dark green bars). Here, the mean of this Poisson distribution is  $\lambda = 2.1$ . The probability distribution of the initial viral population size being  $N$ , conditional on successful infection, is also shown (light green bars). **B)** Proportion of simulated infections that resulted in  $k = 0, 1, 2, \dots$  clonal

variants (dark green bars). Of the 100 simulated infections, 78 recipients had no clonal variants, 12 recipients had 1 clonal variant, 7 recipients had 2 clonal variants, 1 recipient had 3 clonal variants, 1 recipient had 5 clonal variants and 1 recipient had 7 clonal variants. Alongside the simulated (observed) data, we show the proportion of infections with  $k = 0, 1, 2, \dots$  clonal variants that we estimated using maximum likelihood values  $\lambda = 2.3$  and  $\mu = 0.39$  (light green bars). **C)** Probabilities of observing  $k = 0$  clonal variants across a range of  $N$  and  $\mu$  values. **D)** Probabilities of observing  $k = 1$  clonal variant across a range of  $N$  and  $\mu$  values. **E)** Probabilities of observing  $k = 2$  clonal variants across a range of  $N$  and  $\mu$  values. **F)** Log-likelihood plot, showing the  $\log(\text{probability})$  of observing the mock dataset given parameters  $\lambda$  and  $\mu$ . Black lines show the true values of  $\lambda$  and  $\mu$ . Dashed red lines show the maximum likelihood values of  $\lambda$  and  $\mu$ . **G)** Log-likelihood plot, as in panel F, with the results plotted as a function of  $\bar{N}$  and  $\mu$ . **H)** Log-likelihood plot, as in panel F, with the results plotted as a function of  $\bar{N}_b$  and  $\mu$ . In F–H),  $R_0$  was set to its true value of 1.6. **I)** Log-likelihood plot, showing the  $\log(\text{probability})$  of observing the mock dataset given parameters  $\lambda$  and  $R_0$ . Black lines show the true values of  $\lambda$  and  $R_0$ . Dashed red lines show the maximum likelihood values of  $\lambda$  and  $R_0$ . **J)** Log-likelihood plot, as in panel I, with the results plotted as a function of  $\bar{N}$  and  $R_0$ . **K)** Log-likelihood plot, as in panel I, with the results plotted as a function of  $\bar{N}_b$  and  $R_0$ . In I–K), the mutation rate was set to its true value of 0.4 mutations per genome per infection cycle. In F–K), log-likelihood values are shown only for the parameter combinations that fall within the 95% confidence region.

For each of these 100 simulated successful infections, we calculated the number of clonal variants present in the recipient viral population once large. Figure 3B shows the proportion of these 100 simulations that resulted in  $k = 0, 1, 2, \dots$  clonal variants. We then set  $R_0$  to its true value of 1.6 and attempted to jointly estimate  $\lambda$  and  $\mu$  from this observed mock dataset. To do this, we first calculated across combinations of  $N$  and  $\mu$  the probability of observing  $k = 0$  clonal variants (Fig. 3C),  $k = 1$  clonal variant (Fig. 3D),  $k = 2$  clonal variants (Fig. 3E),  $k = 3$  clonal variants (not shown),  $k = 5$  clonal variants (not shown), and  $k = 7$  clonal variants (not shown). We did not perform the calculation for other values of  $k$  because there were no simulated infections that resulted in these other numbers of clonal variants.

From the mock dataset shown in Fig. 3B, our goal was then to estimate  $\lambda$  and  $\mu$  given knowledge of the within-host basic reproduction number  $R_0$ . To do this, we first adjusted the Poisson distribution shown in Fig. 3A (dark green bars) to reflect the distribution of initial viral population sizes we would expect across successful infections (Fig. 3A, light green bars). This adjustment involved multiplying the Poisson probability masses by the  $N$ -specific probabilities

of successful establishment  $(1 - (1/R_0)N)$  and renormalizing. For a given transmission pair, the probability that a recipient's viral population harbors  $k$  clonal variants is then given by

$$\text{Prob}(k|\lambda, \mu, R_0) = \sum_{N=0}^{\infty} p_N(\lambda) \rho_k(N, \mu, R_0),$$

where  $p_N(\lambda)$  is the probability that  $N$  viral particles started off a successful viral infection under an assumed Poisson distribution with mean  $\lambda$  (Fig. 3A, light green bars) and  $\rho_k(N, \mu, R_0)$  is the probability that the recipient's viral population harbors  $k$  clonal variants. We can calculate this probability for each of the 100 transmission pairs in our mock dataset, and then calculate the overall log-likelihood of observing the data shown in Fig. 3B (dark green bars) by summing the log of these probabilities. In Fig. 3F, we plot this log-likelihood surface over a broad range of  $\lambda$  values and  $\mu$  values, while setting the within-host basic reproduction number  $R_0$  to its true value of 1.6. The estimated values of  $\mu$  and  $\lambda$  are very close to their true values and the 95% confidence intervals include the true value. As such, these results indicate that our inference approach performs well on this simulated dataset of 100 transmission pairs.

In addition to plotting the log-likelihood landscape as a function of  $\lambda$  and  $\mu$ , we can plot the same results as a function of the mean realized initial viral population size  $\bar{N}$  and  $\mu$  (Fig. 3G). The mean realized initial viral population size quantifies the mean number of initial viral particles across successful infections and as such corresponds to the mean of the adjusted Poisson distribution shown in Fig. 3A (light green bars). The mean initial viral population size is given by

$$\bar{N} = \sum_{N=0}^{\infty} N p_N(\lambda).$$

Similarly, we can plot the log-likelihood landscape as a function of the mean transmission bottleneck size  $\bar{N}_b$  and  $\mu$  (Fig. 3H). The expression for the mean transmission bottleneck size is provided in the Supplementary Material. The mean transmission bottleneck size quantifies the mean number of initial viral particles that successfully establish genetic lineages in the recipient host.

Finally, we can use our maximum likelihood estimates of  $\lambda$  and  $\mu$  to generate the predicted probability distribution for the number of clonal variants observed. We generate this estimated distribution using equation (1). Figure 3B shows this estimated distribution (light green bars) alongside the distribution from the simulated dataset (dark green bars). These distributions are quantitatively similar, indicating that our model, as parameterized, can recover the distribution of clonal variant outcomes observed in the mock dataset.

In the above analysis, we fixed  $R_0$  at its true value of 1.6 and jointly estimated  $\mu$  and  $\lambda$ . In a specific application to data, it might be the case that a literature estimate exists for  $\mu$  but not the within-host basic reproduction number. We therefore assessed whether we could accurately infer within-host  $R_0$  alongside  $\lambda$  while fixing  $\mu$  at its true value of 0.4 mutations per genome per infection cycle. We found that our maximum likelihood estimates of  $R_0$  and  $\lambda$  were again very close to their true values and that the true values of  $R_0$  and  $\lambda$  again fell within our 95% confidence interval. However, the 95% confidence interval of  $\lambda$ , our primary parameter of interest, was considerably broader than when we set  $R_0$  to its true value and jointly estimated  $\mu$  and  $\lambda$  (Fig. 3I). Figure 3J and K, respectively, show these results as a function of  $\bar{N}$  and  $\bar{N}_b$  instead of  $\lambda$ .

Finally, we asked whether it would be possible to jointly estimate  $\lambda$ ,  $\mu$ , and  $R_0$  based on the number of observed clonal variants across the mock dataset of transmission pairs. Supplementary

figure S2A–C shows the profile likelihoods for  $\lambda$ ,  $R_0$ , and  $\mu$ , respectively, over broad ranges. The profile likelihoods are remarkably flat, with the 95% confidence intervals on each of these parameters spanning across the shown ranges. These flat likelihood curves indicate that there are identifiability issues that arise when trying to jointly estimate all 3 of these parameters. To better understand why this is the case, we jointly estimated  $\mu$  and  $\lambda$  while setting the within-host  $R_0$  to different values: 1.3 (supplementary fig. S2D), 1.6 (the true value; supplementary fig. S2E), and 3 (supplementary fig. S2F). While the maximum likelihood values across these 3 panels are very similar, the maximum likelihood estimates for  $(\lambda, \mu)$  transition from a high  $\lambda$ , low  $\mu$  combination at low  $R_0$  to a low  $\lambda$ , high  $\mu$  combination at high  $R_0$ . These results make sense in that a low  $R_0$  results in a higher mean number of clonal variants (Fig. 2A and B). For a specific dataset, this leads to lower  $\mu$  values and higher  $\lambda$  values, both of which tend to decrease the number of clonal variants observed. Analogously, a high  $R_0$  results in a lower mean number of clonal variants (Fig. 2A and B). For a specific dataset, this leads to higher  $\mu$  values and lower  $\lambda$  values, both of which tend to increase the number of clonal variants observed. Taken together, the results in supplementary fig. S2 therefore indicate that either the mutation rate or the within-host  $R_0$  needs to be set to a reasonable value based on literature estimates to be able to make informative inferences about transmission bottleneck sizes using this approach.

### ***Application to Empirical Data***

We apply our inference approach to 2 acutely infecting respiratory viruses: seasonal IAV and SARS-CoV-2. Application of our approach to an empirical dataset works analogously to the application of our approach to a simulated dataset. The only additional step involves the identification of clonal variants using virus deep-sequencing data from donor–recipient transmission pairs. Below, we use transmission pairs that have been previously identified using a

combination of epidemiological, clinical, and viral genetic criteria. We identify clonal variants in these already-established transmission pairs by first setting a variant-calling threshold (e.g. 3%). We then call intrahost single nucleotide variants (iSNVs) for the donor sample and for the recipient sample based on this threshold. All sites that harbor an iSNV in either the donor or the recipient are then removed from consideration, as they are polymorphic in at least one of these individuals. At the remaining sites, we determine which allele is present in both the donor and the recipient. Any site that carries a different allele in the recipient compared to the donor is then called as a clonal variant.

### ***Application to IAV***

As the first empirical application of our inference approach, we considered a rich IAV dataset from a prospective community-based cohort study (McCrone et al. 2018). The relevant portion of this dataset are 52 transmission pairs that were identified as part of this study (Supplementary Material). For each of these transmission pairs, we calculated the number of clonal variants observed in the recipient using a variant-calling threshold of 3%. The data consisted of 42 transmission pairs with 0 clonal variants, 5 transmission pairs with 1 clonal variant, 2 transmission pairs with 2 clonal variants, 3 transmission pairs with 3 clonal variants, and 0 transmission pairs with 4 or more clonal variants (Fig. 4A). We set the within-host basic reproduction number  $R_0$  to 11.1, based on a quantitative analysis of IAV dynamics in longitudinally studied human IAV infections (Baccam et al. 2006). We considered  $\lambda$  values in the range of  $(0, 4]$  mean initial viral particles and  $\mu$  values between 0 and 3.5 mutations per genome per infection cycle. In practice, we considered a range in  $\lambda$  from 0.01 to 4 mean initial viral particles and then also evaluated the limit as  $\lambda$  approached 0 by calculating the likelihood with  $N = 1$  initial viral particles.

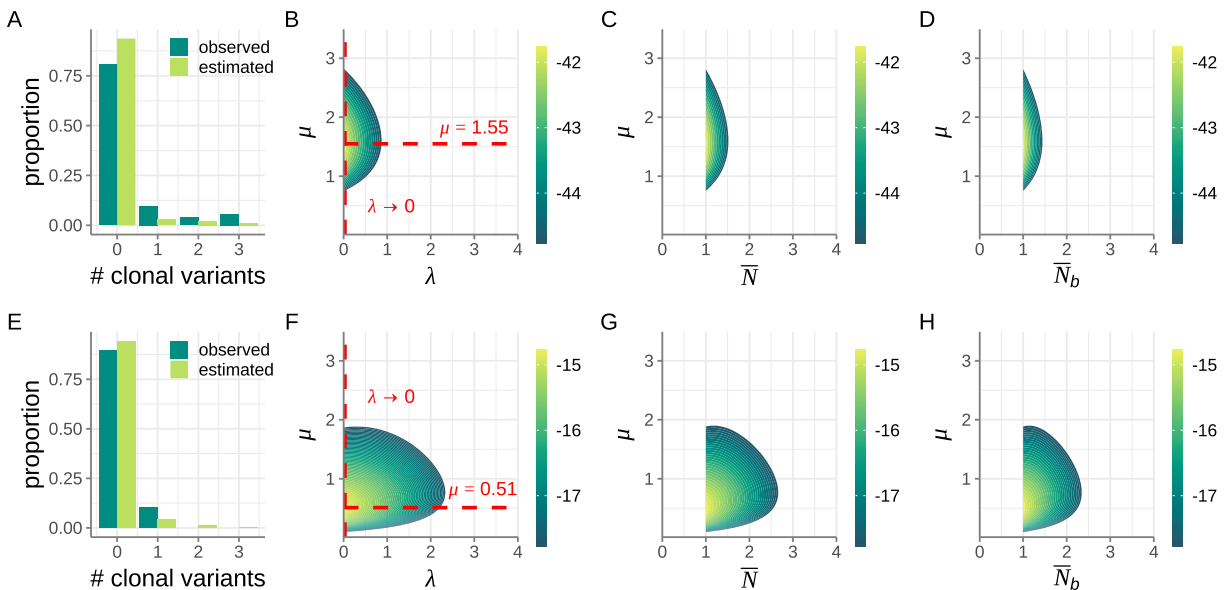


**Fig. 4. Application of our inference method to IAV and SARS-CoV-2 transmission pairs.** Top row shows IAV results. Bottom row shows SARS-CoV-2 results. **A)** Distribution of the number of clonal variants observed across the 52 identified IAV transmission pairs (dark green bars). The expected distribution under the maximum likelihood estimates of  $\lambda$  and  $\mu$  (light green bars) is shown alongside the empirical distribution. **B)** Log-likelihood plot, showing the log(probability) of observing the IAV dataset across a range of  $\lambda$  and  $\mu$  values. Dashed red lines show the maximum likelihood values for  $\lambda$  and  $\mu$ . The value of  $\lambda \rightarrow 0$  was evaluated by assuming that 100% of successful transmissions started off with  $N = 1$  initial viral particles. **C)** Log-likelihood plot, as in panel B, with the results plotted as a function of  $\bar{N}$  and  $\mu$  instead of  $\lambda$  and  $\mu$ . **D)** Log-likelihood plot, as in panel B, with the results plotted as a function of  $\bar{N}_b$  and  $\mu$  instead of  $\lambda$  and  $\mu$ . The 95% confidence region of  $\bar{N}_b$  spanned the range [1.00, 1.41]. **E)** Distribution of the number of clonal variants observed across the 39 identified SARS-CoV-2 transmission pairs (dark green bars). The expected distribution under the maximum likelihood estimates of  $\lambda$  and  $\mu$  (light green bars) is shown alongside the empirical distribution. **F)** Log-likelihood plot, showing the log(probability) of observing the SARS-CoV-2 dataset across a range of  $\lambda$  and  $\mu$  values. **G)** Log-likelihood plot, as in panel F, with the results plotted as a function of  $\bar{N}$  and  $\mu$  instead of  $\lambda$  and  $\mu$ . **H)** Log-likelihood plot, as in panel F, with the results plotted as a function of  $\bar{N}_b$  and  $\mu$  instead of  $\lambda$  and  $\mu$ . The 95% confidence region of  $\bar{N}_b$  spanned the range [1.00, 2.31]. In panels B–D and F–H, only the log-likelihood values that fall within the 95% confidence region are shown.

Figure 4B shows the log-likelihood surface for  $\lambda$  and  $\mu$ . Figure 4C and D plots these same results as a function of  $\bar{N}$  and  $\bar{N}_b$ , respectively. The log-likelihood surface shown in Fig. 4D corroborates previous results of very tight transmission bottlenecks for IAV (McCrone et al. 2018). Indeed, the maximum likelihood estimate of  $\lambda \rightarrow 0$  indicates that almost all successful transmissions are predicted to have started with a single initial viral particle ( $N = 1$ ). Our results



further provide an estimate of the mutation rate that is consistent with an independent mutation rate estimate obtained using a twelve class fluctuation test (Pauly et al. 2017). Specifically, the fluctuation test estimated the occurrence of 2 to 3 mutations on average per replicated genome. With approximately 30% of IAV mutations estimated to be lethal deleterious (Visher et al. 2016), we expect based on these results that  $\mu$  be approximately  $(2 - 3) \times 0.70 = 1.4 - 2.1$  mutations per replicated genome, consistent with our findings in Fig. 4B–D. Finally, we used our maximum likelihood estimates of  $\lambda$  and  $\mu$  to generate the predicted probability distribution for the number of clonal variants observed. Figure 4A shows this predicted distribution alongside the distribution from the empirical IAV dataset. Although the predicted and empirical distributions are quantitatively similar, we note that our model, parameterized with maximum likelihood parameter values, appears to overestimate the proportion of clonal variants in the  $k = 0$  class and underestimate the proportion of clonal variants in higher- $k$  classes.

Because our findings depend on our assumption of  $R_0$ , we reapplied our inference approach across a broader range of reasonable  $R_0$  values. Supplementary figure S3 provides a sensitivity analysis of our  $\lambda$  and  $\mu$  estimates under a range of  $R_0 = 4.4$  to  $37.7$ , corresponding to the minimum and maximum  $R_0$  estimates in Baccam et al. (2006). This analysis indicates that our estimates are relatively insensitive to the exact value of  $R_0$  assumed. Across the range of  $R_0$  values considered, the maximum likelihood estimates of  $\lambda$  and associated mean transmission bottleneck sizes  $\bar{N}_b$  remained low. The maximum likelihood estimates of the mutation rate also remained at similar values, with a slightly lower mutation rate estimated when  $R_0$  was assumed to be low compared to when it was assumed to be high. Of note, the overestimation of the probability mass in the  $k = 0$  class (and the underestimation of the probability masses in the  $k \geq$

1 classes) is less stark at lower  $R_0$  values, indicating that literature estimates of within-host  $R_0$  values may be high.

Because our sensitivity analyses indicate that the clonal variant data may support an  $R_0$  value that is lower than current literature estimates, we decided to perform an additional analysis where we set the mutation rate and attempted to instead jointly estimate  $\lambda$  and the within-host basic reproduction number  $R_0$  (supplementary fig. S4A–D). With this analysis, we found that the maximum likelihood estimate for within-host IAV  $R_0$  was 5.01, while the maximum likelihood estimate for  $\lambda$  remained at  $\lambda \rightarrow 0$ , corresponding to all successful transmissions starting off with a single initial viral particle ( $N = 1$ ). The maximum likelihood estimate of within-host  $R_0 = 5.01$  is low compared to the range of individual estimates given in Baccam et al. (2006), although one of the 6 individuals studied in that analysis had an  $R_0$  estimate lower than 5.01. As an additional consideration, the within-host  $R_0$  we estimated in supplementary fig. S4 reflects the value of this parameter very early on during the infection process, while the within-host  $R_0$  estimated in Baccam et al. (2006) is based on the exponential growth rate of the viral population once viral titers are sufficiently high to be detected with nasal washes. Due to changes in cellular multiplicities of infection over this period, and the effect this would have on viral complementation and competition, it might be the case that these within-host  $R_0$  values are not immediately comparable.

### ***Application to SARS-CoV-2***

Next, we applied our inference approach to a previously published SARS-CoV-2 transmission pair dataset from Austria (Popa et al. 2020). This dataset included 39 identified transmission pairs from early on in the SARS-CoV-2 pandemic (Supplementary Material). Based on shared genetic variation between donors and recipients, transmission bottlenecks sizes were

estimated to be tight (Martin and Koelle 2021; Nicholson et al. 2021), on the order of 1–3 viral particles. Here, we reanalyzed these same transmission pairs using our new inference approach, again using a variant-calling threshold of 3%. The data consisted of 35 transmission pairs with 0 clonal variants, 4 transmission pairs with 1 clonal variant, and 0 transmission pairs with 2 or more clonal variants (Fig. 4E). We set the within-host basic reproduction number  $R_0$  to 7.4, based on a quantitative analysis of SARS-CoV-2 dynamics in longitudinally studied human SARS-CoV-2 infections (Ke et al. 2021). We again considered  $\lambda$  values in the range of (0, 4] initial viral particles and  $\mu$  values between 0 and 3.5 mutations per genome per infection cycle.

Figure 4F shows the log-likelihood surface for  $\lambda$  and  $\mu$ . Figure 4G and H plots these same results as a function of  $\bar{N}$  and  $\bar{N}_b$ , respectively. The log-likelihood surface shown in Fig. 4H corroborates previous results of very tight transmission bottlenecks for SARS-CoV-2 (Braun et al. 2021b; Lythgoe et al. 2021; Martin and Koelle 2021; Nicholson et al. 2021; Bendall et al. 2023). It further provides an estimate of the mutation rate that is largely consistent with an independent mutation rate estimate of  $1 - 5 \times 10^{-6}$  per site per infection cycle (Amicone et al. 2022). This estimate translates to a mutation rate of approximately 0.03 to 0.15 mutations per genome per infection cycle. Again, with approximately 30% of these mutations likely being lethal deleterious, we expect  $\mu$  to be approximately 0.02 to 0.10 mutations per infection cycle. While our maximum likelihood estimate of  $\mu = 0.52$  exceeds this estimated range, our 95% confidence interval on  $\mu$  extends into this range. Finally, we used our maximum likelihood estimates of  $\lambda$  and  $\mu$  to again generate the predicted probability distribution for the number of clonal variants observed. Figure 4E shows this predicted distribution alongside the distribution from the empirical SARS-CoV-2 dataset. We again note that while the predicted and estimated distributions are quantitatively similar, our maximum likelihood parameter estimates appear to

overestimate the proportion of clonal variants in the  $k = 0$  class, and underestimate the proportion of clonal variants in higher- $k$  classes.

To determine the sensitivity of our findings to our assumption of  $R_0 = 7.4$ , we again reapplied our inference approach across a broader range of reasonable  $R_0$  values. Supplementary figure S5 shows our results under a range of  $R_0$  values that span 2.6 to 14.9, corresponding to the minimum and maximum  $R_0$  estimates in Ke et al. (2021). Our results again indicate that our estimates are relatively insensitive to the exact value of  $R_0$  assumed. As was the case with our IAV analysis, estimates of  $\mu$  were slightly higher at higher within-host  $R_0$  values. Again, the overestimation of the probability mass in the  $k = 0$  class (and the underestimation of the probability masses in the  $k \geq 1$  classes) is reduced at lower  $R_0$  values, again indicating that literature estimates of within-host  $R_0$  values may be high.

As we did for the IAV dataset, we then again considered an alternative analysis where we set the mutation rate to an estimate from the literature and attempted to instead jointly estimate  $\lambda$  and the within-host basic reproduction number  $R_0$  (supplementary fig. S4E–H). With this analysis, we found that the maximum likelihood estimate for within-host SARS-CoV-2  $R_0$  was 1.21, while the maximum likelihood estimate for  $\lambda$  remained at  $\lambda \rightarrow 0$ .

### ***Guarding Against the Erroneous Calling of Clonal Variants***

In our application to empirical data, our findings will depend not only on the assumed value of  $R_0$  but also on the variant-calling threshold used. In particular, a lower variant-calling threshold has the potential to reduce the number of clonal variants called. This would occur if a site (in either the donor, the recipient, or both) goes from being called a clonal variant at a higher variant-calling threshold to being excluded from consideration at a lower variant-calling threshold because this former clonal variant is now instead called as an iSNV in one or both

individuals. This brings us to the question of which variant-calling threshold should be used and how we can best guard against the erroneous calling of clonal variants when they might be transmitted from a donor instead of arising *de novo* in a recipient host. Here, we provide several approaches that can be used to address these concerns and to thereby assess the robustness of our conclusions.

The first approach is simply to perform a sensitivity analysis that uses different variant-calling thresholds to calculate the number of clonal variants in each of the identified transmission pairs. To provide an example of this approach, we recalled clonal variants for the IAV and SARS-CoV-2 datasets at variant-calling thresholds of 0.5% and 7% (supplementary figs. S6 and S7). As anticipated, the number of clonal variants observed was lower at the 0.5% variant-calling threshold than at the 3% threshold and the number of clonal variants observed was higher at the 7% variant-calling threshold than at the 3% threshold. This was the case for both datasets. For the IAV dataset, neither the maximum likelihood estimate for  $\mu$  nor the maximum likelihood estimate for  $\lambda$  was sensitive to the specific variant-calling threshold used. Furthermore, the 95% confidence interval did not change dramatically across the thresholds evaluated (supplementary fig. S6). For the SARS-CoV-2 dataset, neither the maximum likelihood estimate for  $\mu$  nor the maximum likelihood estimate for  $\lambda$  was sensitive to the specific variant-calling threshold used. The 95% confidence interval, however, did broaden at the lower variant-calling threshold of 0.5% (supplementary fig. S7). Overall, this sensitivity analysis provides reassurance that our findings are largely robust to changes in the variant-calling threshold used.

The second approach is to examine the empirical frequencies of the clonal variants called at a given variant-calling threshold. If a clonal variant is present at 0% in a donor and present at 100% in a recipient, then it is very likely that it arose *de novo* within the recipient and spread to

fixation within that individual (although we cannot exclude the possibility that this variant was present as an iSNV in the donor at the time of transmission but was present in 0% of donor reads at the time of sampling). If a clonal variant is present at 0% in a donor and close to 100% (but not fixed) in the recipient, it is likely that the clonal variant arose de novo in the recipient but had not quite yet fixed in the recipient by the time of sampling. In this case, we may want to keep on considering this variant as a clonal variant. Finally, if a clonal variant is observed at a frequency above 0% in the donor (regardless of whether it is fixed or close to fixation in the recipient), we may want to be more cautious about calling this variant a clonal variant. This is because the donor may have transmitted this iSNV to the recipient. Based on these considerations, we revisited both of the empirical datasets. In the IAV dataset, of the 18 clonal variants identified at the 3% variant-calling threshold, 12 were present at frequencies of 0% in the donor and 100% in the recipient. Five were present at frequencies of 0% in the donor and  $\geq 99.1\%$  in the recipient. The remaining variant was present at 2.3% frequency in the donor and fixed at 100% in the recipient. We therefore considered an additional analysis where we included only the 17 clonal variants that were present in the donor at 0% frequency. This analysis resulted in similar estimates of  $\mu$  and  $\lambda$  as in our original analysis (supplementary fig. S8). In the SARS-CoV-2 dataset, of the 4 clonal variants identified at the 3% variant-calling threshold, 3 were present at frequencies of 0% in the donor and  $\geq 98.6\%$  in the recipient. The remaining variant was present at 0.7% frequency in the donor and at 99.9% in the recipient. We therefore considered an additional analysis where we included only the 3 clonal variants that were present in the donor at 0% frequency. Again, this analysis resulted in similar estimates of  $\mu$  and  $\lambda$  as in our original analysis (supplementary fig. S9).

Finally, we would like to note that if an iSNV that was present at very low frequency in the donor was transmitted and observed as fixed in the recipient, this would itself point toward a very small transmission bottleneck. This is because the probability of a low-frequency iSNV being transmitted and fixing in the recipient is higher at low  $N$  than at high  $N$  (Supplementary Material; supplementary fig. S10). As such, even if a variant was erroneously called as a clonal variant when it was instead a low-frequency donor iSNV that was transmitted, its presence would consistently point toward a small transmission bottleneck size.

### ***Considering Alternative Distributions for the Initial Number of Viral Particles That Start an Infection***

In our analysis of the mock dataset as well as in our analysis of the empirical IAV and SARS-CoV-2 datasets, we assumed that the initial number of viral particles  $N$  was Poisson-distributed. This assumption is consistent with an underlying process in which viral particles are transmitted from a donor at a constant rate during a contact event with fixed duration time. However, because of variation in the amount of virus a donor expels or because of differences in contact duration or transmission routes, a Poisson distribution for the number of initial viral particles might not be a good assumption. We therefore considered 2 alternative distributions for the initial number of viral particles. We first considered a highly over-dispersed negative binomial distribution for  $N$ , with a large proportion of recipients receiving only very few initial viral particles and a small proportion receiving many initial viral particles, such that the variance of the distribution greatly exceeds its mean. Assuming this distribution, we attempted to jointly estimate its mean ( $\lambda_{NB}$ ) and the mutation rate  $\mu$  while setting the overdispersion parameter to a small value ( $k = 0.1$ ). For both the IAV and SARS-CoV-2 datasets, we found that the mean of this negative binomial distribution was low, similar to our findings using the Poisson distribution

(Fig. 5B and E). We next considered a model in which a proportion  $p$  of recipients received  $N = 1$  viral particles from their donors, while the remaining proportion  $(1 - p)$  received a large number of viral particles from their donors. We assumed that the number of initial viral particles in the latter recipients was so large that none of them would harbor a clonal variant. For both IAV and SARS-CoV-2 datasets, we found that the proportion of recipients receiving  $N = 1$  initial viral particles was very high (Fig. 5C and F). These additional analyses indicate that, while we do not know the underlying initial distribution of viral particles that recipients begin with, the pattern of clonal variants observed across transmission pairs points toward a large fraction of infected recipients starting their infection off with a very small number of initial viral particles. This does not exclude the possibility that a small fraction of infected recipients had their infections start off with a large number of initial viral particles, due to either contact with a donor that expelled a large amount of virus, a very long contact with a donor, or a contact of a specific type that could result in a large number of initial viral particles in the recipient.



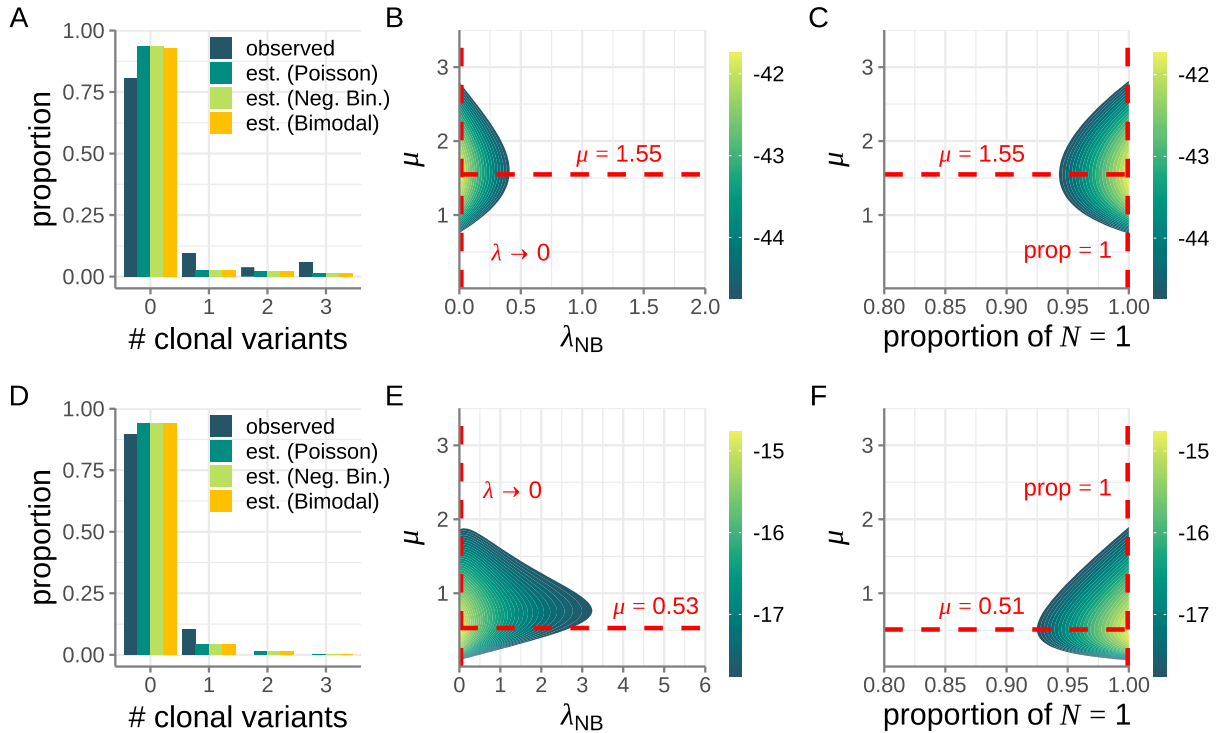


**Fig. 5. Consideration of alternative distributions for the number of initial viral particles  $N$ .** Top row shows IAV results. Bottom row shows SARS-CoV-2 results. **A)** Distribution of the number of clonal variants observed across the 52 IAV transmission pairs considered (dark green bars). The expected distributions using the IAV maximum likelihood parameter estimates are shown in green, light green, and orange bars, respectively, for the Poisson distribution, negative binomial distribution, and bimodal ( $N = 1$  or  $N$ -large) distribution. **B)** Log-likelihood plot, showing the log(probability) of observing the IAV dataset across a range of  $\lambda_{NB}$  and  $\mu$  values. Dashed red lines show the maximum likelihood values for  $\lambda_{NB}$  and  $\mu$ . The parameter  $\lambda_{NB}$  quantifies the mean of the negative binomial distribution. The overdispersion parameter of the negative binomial distribution was set to  $k = 0.1$ . **C)** Log-likelihood plot, showing the log(probability) of observing the IAV dataset across a range of  $p$  and  $\mu$  values. Dashed red lines show the maximum likelihood values for  $p$  and  $\mu$ . The parameter  $p$  quantifies the proportion of recipients that start their infection off with  $N = 1$  initial viral particles. **D)** Distribution of the number of clonal variants observed across the 39 SARS-CoV-2 transmission pairs considered (dark green bars). The expected distributions using the SARS-CoV-2 maximum likelihood parameter estimates are shown in green, light green, and orange bars, respectively, for the Poisson distribution, negative binomial distribution, and bimodal distribution. **E)** Log-likelihood plot, showing the log(probability) of observing the SARS-CoV-2 dataset across a range of  $\lambda_{NB}$  and  $\mu$  values. Dashed red lines show the maximum likelihood values for  $\lambda_{NB}$  and  $\mu$ . The overdispersion parameter of the negative binomial distribution was set to  $k = 0.1$ . **F)** Log-likelihood plot, showing the log(probability) of observing the SARS-CoV-2 dataset across a range of  $p$  and  $\mu$  values. Dashed red lines show the maximum likelihood values for  $p$  and  $\mu$ . For both datasets, a 3% variant-calling threshold was used to call clonal variants.

## Discussion

Here, we developed a new statistical approach for estimating transmission bottleneck sizes from viral deep-sequencing data from donor–recipient transmission pairs. This approach differs from previous approaches in that it does not use the subset of viral sites that are identified as polymorphic in the donor. Instead, our approach relies on the number of clonal variants observed in the recipient. Observed clonal variants arise *de novo* shortly after transmission and are particularly well suited for estimating bottleneck sizes when bottlenecks are likely to be tight.

Our approach carries several advantages over existing approaches. First, transmission pairs where the donor does not show any genetic variation are still informative and can be included in our analysis. Second, a misspecification of donor versus recipient in a transmission pair does not impact results, as the number of clonal variants is the same with a correct donor/recipient assignment or the reverse. Third, existing studies that have looked at longitudinal viral samples have indicated that variant frequencies are highly dynamic over the course of an acute infection, consistent with a small within-host effective population size. As such, variant frequencies from a donor sample that are used to estimate bottleneck sizes may not reflect variant frequencies present in the donor at the time of transmission, and would lead to underestimates of  $N_b$ . Even if bottleneck sizes were large, changes in variant frequencies due to genetic drift in recipients would similarly bias  $N_b$  estimates to be low. In contrast, our approach does not rely on variant frequencies in a donor, nor does it rely on variant frequencies in a recipient. As such, it is not subject to these same biases. Examination of our datasets also indicates that clonal variants remain clonal over the course of a recipient's infection, such that the timing of the sampling event does not impact our dataset and thus does not impact our bottleneck size estimates. Finally,

if viral particles from a donor are not randomly sampled, this does not impact our inference, while it would again bias  $N_b$  estimates to be low with existing inference approaches.

Despite these advantages of our new inference approach, there are some limitations to it. First, estimation of transmission bottleneck sizes requires more than a single transmission pair. Second, our approach depends on a very limited subset of the donor and recipient deep-sequencing data. However, for the reasons we described above, we do not believe that patterns of shared genetic variation between the donor and the recipient are particularly informative of transmission bottleneck sizes, at least for acute viral respiratory infections such as influenza and SARS-CoV-2. Our approach does ignore de novo genetic variation that is subclonal in the recipient, however (that is, de novo variants that are called in a recipient but are not fixed). Our approach could, in principle, be extended to accommodate these variants. However, based on longitudinal analyses of IAV infections (McCrone et al. 2018), we also think that many of these subclonal variants come and go over the course of an infection, such that they are not informative of the transmission bottleneck size, but instead are more informative of the extent of genetic drift that occurs over the course of an acute infection. We thus do not recommend extension of our approach to accommodate subclonal variants. Additional limitations of our approach include our assumption of infinite sites and our assumption that all genetic variation is neutral. We do not believe that the infinite sites assumption would substantially bias our results because the number of clonal variants is very small compared to the length of the viral genome. We also do not believe that the neutrality assumption would substantially bias our results in the case of small transmission bottleneck sizes because genetic drift dominates in this regime, such that small fitness differences between viral particles will not impact the viral population's

evolutionary dynamics. Lethal deleterious mutations will simply act to lower the mutation rate estimate or decrease the effective within-host  $R_0$  of the viral population.

Finally, our approach assumes complete genetic linkage across the viral genome. Again, we do not believe that this assumption would bias our results substantially, for several reasons. First, previous work has indicated that the effective rate of reassortment in human IAV infections is low even when viral titers are high (Sobel Leonard et al. 2017a), potentially due to spatial structure in the respiratory tract. As such, even if reassortment or recombination for viral respiratory pathogens is common, this genetic exchange likely occurs between genetically identical viral haplotypes and would therefore not bias our bottleneck size estimates that assume that linkage is complete. Second, if a mutation arises de novo in a recipient and fixes, this is very likely to occur within the first few viral replication cycles when the extent to which viral genetic diversification has occurred is limited and while viral population sizes in the recipient are still very small. Because of the small population sizes during this time period, the probability of high cellular multiplicity of infection may also be lower, and as such, the probability that recombination or reassortment occurs may be lower. If recombination or reassortment did occur early on during an infection, however, it could allow 2 mutations that arose de novo in different genetic backgrounds to come into the same background, allowing both to fix when in the absence of recombination/reassortment, neither would fix. By not considering this possibility, our estimate of  $N_b$  would be biased low because we would ascribe the observation of 2 clonal variants in a recipient to be due to a small bottleneck rather than recombination/reassortment in the context of a larger bottleneck. Again, we think that the occurrence of this scenario is extremely rare, given that effective rates of recombination are likely to be low and that

recombination/reassortment would have to occur very early on during infection when viral population sizes were still very small.

In our application to influenza A virus and to SARS-CoV-2, we found that transmission bottleneck sizes were very tight, consistent with previous findings of small  $N_b$ . This is an important finding, given that previous methods, as elaborated on above, are likely to underestimate bottleneck sizes due to within-host genetic drift and the potential for viral aggregation during the transmission process. That both this new approach and existing approaches arrive at the conclusion of very small bottleneck sizes does not lessen the advantage of using this new approach over existing approaches. If bottleneck sizes were large, and existing methods were considerably underestimating them, the IAV and SARS-CoV-2 datasets would not have contained any clonal variants. Our new approach would have indicated that for reasonable  $\mu$  and within-host  $R_0$  values, we would have anticipated observing clonal variants in a subset of the transmission pairs if bottleneck sizes were small. Their absence would therefore have argued against small bottleneck sizes and would have pointed toward previous methods indeed yielding biased estimates. That both sets of approaches (those based on shared genetic variation and the current one based on de novo clonal variants) infer very small transmission bottlenecks provides compelling evidence that these bottlenecks for acutely infecting respiratory viral pathogens are indeed incredibly small. This raises the question of what environmental and molecular mechanisms constrain transmission bottleneck sizes. Are the number of viral particles that reach the respiratory tract of a recipient limited? Or do many viral particles reach a recipient's respiratory tract but host and/or viral factors limit the number of viral lineages that establish? Our results of tight transmission bottleneck sizes for IAV and SARS-CoV-2 also indicate that reductions in viral population sizes between transmission events will have a large impact on

shaping these viruses' patterns of evolution and adaptation at the population level. Will these small bottlenecks ultimately act to impede viral adaptation or to facilitate it? And how will these tight bottlenecks impact population-level viral patterns, including patterns of antigenic change, genetic diversification, and deleterious mutation loads? Addressing these questions through theoretical and empirical studies will facilitate our understanding of viral transmission dynamics and ultimately guide our ability to curb the spread of these infectious diseases.

## Supplemental Material

### *Derivation of the probability distribution for the number of clonal variants*

Here, we derive the probabilities associated with the possible dynamic outcomes shown in Figure 1E and then show how these probabilities can then be used to obtain the probability distribution for the number of clonal variants. Consider first a contact between a donor and a recipient that results in the transfer of  $N$  infectious viral particles. Following this transfer, the within-host dynamics of the viral population depend on the within-host basic reproduction number  $R_0$ .

Because the initial viral population size may be small, we consider the viral population dynamics to be subject to demographic stochasticity. More specifically, we assume that the viral population undergoes stochastic birth-death dynamics. This is dynamically equivalent to a branching process model with a geometric offspring distribution parameterized with a success probability of  $p_{geom} = 1/(R_0 + 1)$ , where  $R_0$  is the mean number of offspring produced (Lloyd-Smith et al., 2005). When  $R_0 < 1$ , this corresponds to the subcritical case, and the viral population will die out with probability 1. In terms of the possible dynamic outcomes in Figure 1E, this corresponds to  $P_X = 1$ , regardless of the initial viral population size  $N$ . When  $R_0 > 1$ ,

this corresponds to the supercritical case. In this case, the viral population still has the possibility of going stochastically extinct. This occurs with probability:

$$P_{X,n=N} = \left(\frac{1}{R_0}\right)^N$$

The probability of the viral population dying out  $P_X$  is the same as the probability of there being no mutant lineages that establish in the viral population ( $S_0$ ), and corresponds to the scenario depicted in Figure 1A.

Because  $P_X = 1$  in the subcritical case of  $R_0 < 1$ , we consider the remaining dynamic outcomes shown in Figure 1E only in the supercritical case. We can next derive the probability that the wild-type viral lineage successfully establishes (labeled  $S_\infty$ ), corresponding to the scenario depicted in Figure 1B. To calculate this probability, we have to consider the rate at which mutations occur during replication in the viral population. We assume a per genome, per infection cycle mutation rate  $\mu$ , with the number of mutations occurring during the production of a viral progeny being Poisson-distributed with this mean. Given this assumption, the probability that a mutation does not occur during the production of a viral progeny is given by  $e^{-\mu}$  and the probability that one or more mutations occur during the production of a viral progeny is given by  $1 - e^{-\mu}$ . Given this set-up, we can decompose the overall geometric offspring distribution into two separate offspring distributions: that of offspring that are genetically identical to the parent and that of offspring that differ from the parent by at least one mutation (Figure S1A). We define the wild-type offspring distribution as the distribution of offspring from wild-type individuals that are themselves wild-type. We further define the mutant offspring distribution as the distribution of offspring from wild-type individuals that instead carry de novo mutations. The wild-type offspring distribution is given by a negative binomial distribution with parameters  $r_w = e^{-\mu}$  and success probability  $p_{geom}$ . The mutant offspring distribution is given by a negative

binomial distribution with parameters  $r_m = 1 - e^{-\mu}$  and success probability  $p_{geom}$ . If the number of wildtype offspring from a wild-type particle is  $X \sim NB(r_w, p_{geom})$  and the number of mutant offspring from a wild-type particle is  $Y \sim NB(r_m, p_{geom})$ , the overall offspring distribution from a wild-type particle is  $X + Y \sim NB(r_w + r_m, p_{geom}) = NB(1, p_{geom}) = Geom(p_{geom})$ , thereby recovering the assumed overall offspring distribution.

Now that we have the wild-type offspring distribution defined, we can calculate the probability that the wild-type viral lineage establishes. This is given by:

$$S_{\infty, n=N} = 1 - (p_{wtext, n=1})^N$$

where  $p_{wtext, n=1}$  is the probability that a wild-type viral lineage, starting with a single infectious viral particle goes extinct. If the mean number of wild-type offspring (given by  $R_0 e^{-\mu}$ ) exceeds one, this probability can be calculated numerically using equation (4) in Nishiura et al. (2012), using the parameters of the wild-type offspring distribution ( $r_w$  and  $p_{geom}$ ). If the mean number of wild-type offspring is less than one,  $p_{wtext, n=1} = 1$ , and  $S_{\infty, n=N} = 0$ .

Now that we have derived  $S_{\infty, n=N}$  and  $S_{0, n=N}$ , we turn to deriving  $S_{1, n=N}$ ,  $S_{2, n=N}$ ,  $S_{3, n=N}$ , etc. Deriving these probabilities is a bit more involved. Our general approach is to first calculate the final size distribution of wild-type particles, conditional on wild-type lineage extinction, and then to use this final size distribution to generate a probability mass function for the number of mutant lineages generated from the wild-type viral population. From this distribution, we calculate the probability mass function for the number of mutant lineages that establish. This probability mass function gives us  $S_{0, n=N}$ ,  $S_{1, n=N}$ ,  $S_{2, n=N}$ , etc., thus completing our analytical expressions for the possible dynamic outcomes shown in Figure 1E.

To first calculate the final size distribution of wild-type particles, we use previous analytical results derived in Nishiura et al. (2012) and Blumberg and Lloyd-Smith (2013b). For



both the wild-type supercritical case ( $R_0 e^{-\mu} > 1$ ) and the wild-type subcritical case ( $R_0 e^{-\mu} < 1$ ), the final size distribution of the wild-type viral population, starting with one single infectious particle, is given by equation (1) in Blumberg and Lloyd-Smith (2013a) for a branching process model with a negative binomial offspring distribution (here, parameterized with  $r_w$  and  $p_{geom}$ ). For the subcritical case, the probability masses of this distribution add up to 1. For the supercritical case, the probability masses of this distribution add up to  $p_{wtext,n=1}$ . We can thus normalize this latter distribution such that its probability masses add up to 1 (thereby conditioning on wild-type viral lineage extinction). We define this normalized probability distribution as  $f_{n=1}$ . Making use of  $f_{n=1}$ , we can then calculate the final size distribution of wild-type particles starting with  $N$  viral particles ( $f_{n=N}$ ) through recursion:

$$f_{j,n=N} = \sum_{i=1}^{j-1} (f_{i,n=1} \times f_{j-i,n=N-1})$$

with the terminal case being  $f_{j,n=1}$ . Here,  $f_{j,n=N}$  refers to the probability mass of the final size of wild-type particles being  $j$ , given an initial viral population size of  $N$ . Figure S1B shows the probability mass function  $f_{n=N}$ .

Once we have the wild-type final size distribution  $f_{n=N}$  (conditional on wild-type extinction), we can calculate the probability mass function for the number of mutant lineages that were generated directly from the wild-type population prior to its extinction. We can do this calculation using the mutant offspring distribution. Because the mutant offspring distribution is a negative binomial distribution with parameters  $r_m$  and  $p_{geom}$ , if the final size of the wild-type population was  $j$ , then the number of mutant offspring from this wild-type population itself follows a negative binomial distribution with parameters  $(j \times r_m)$  and  $p_{geom}$ . We can thus iterate over all possible wild-type final population sizes to calculate an overall distribution for the

number of mutant viral lineages that are generated from this wild-type population that ultimately goes extinct. We define this overall distribution as  $g_{n=N}$  (Figure S1C).

Finally, we can use  $g_{n=N}$  to calculate the distribution of the number of mutant lineages that establish, which we refer to as  $h_{n=N}$ . Each mutant lineage has a probability of establishing of  $1 - 1/R_0$ , such that:

$$h_{j,n=N} = \sum_{m=0}^{\infty} [(g_{m,n=N}) \times \text{Bin}(j, m, 1 - 1/R_0)]$$

for  $j = 0, 1, 2, \dots$  (Figure S1D). Here,  $\text{Bin}(j, m, 1 - 1/R_0)$  is the binomial probability of observing  $j$  successes, given  $m$  trials and a probability of success of  $1 - 1/R_0$ . We can then calculate  $S_{0,n=N}$ ,  $S_{1,n=N}$ ,  $S_{2,n=N}$ , etc., from  $h_{n=N}$  by:

$$S_{k,n=N} = (h_{k,n=N}) \times (1 - S_{\infty,n=N})$$

where  $k = 0, 1, 2, \dots$  (but not  $\infty$ ). This completes our analytical derivations for the outcomes depicted in Figure 1E.

As shown in Figure 1E, the probability of an infection going stochastically extinct in a recipient is given by:

$$P_{X,n=N} = S_{0,n=N}$$

The probability of there being zero clonal variants observed in a recipient is given by:

$$P_{0,n=N} = \sum_{i=2}^{\infty} S_{i,n=N}$$

The probability of there being 1 or more clonal variants is given by:

$$P_{1+,n=N} = S_{1,n=N}$$

These three probabilities are shown in Figure S1E. We now turn to resolving  $P_{1+,n=N}$  into the probability of observing exactly  $k = 1, 2, 3, \dots$  clonal variants.

Given the mutation rate  $\mu$ , the probability that exactly  $k$  mutations occurred during the production of the mutant lineage is given by:

$$\frac{Poiss(k, \mu)}{1 - Poiss(0, \mu)}$$

where  $Poiss(k, \mu)$  is the Poisson probability of observing  $k$  mutations given a mutation rate of  $\mu$ . To a first approximation, we can therefore write:

$$P_{k,n=N} \approx P_{1+,n=N} \times \left( \frac{Poiss(k, \mu)}{1 - Poiss(0, \mu)} \right)$$

for  $k \geq 1$ . This expression captures the possibility that more than one clonal variant arises during the generation of a mutant lineage from a wild-type particle. However, this expression is an approximation because there is a possibility that additional clonal variants arise following the generation of this mutant lineage (that is, during its establishment). We can correct for this possibility by modifying the above expression by probabilities of these additional clonal variants arising. Specifically, we can write the probability of there being exactly one clonal variant as the product of there being one mutation that occurs during the generation of the first mutant lineage and there being no additional clonal variants arising in this lineage that starts off with one mutant viral particle:

$$P_{1,n=N} = P_{1+,n=N} \times \left( \frac{Poiss(1, \mu)}{1 - Poiss(0, \mu)} \right) \times \left( \frac{P_{0,n=1}}{1 - P_{X,n=1}} \right)$$

We can similarly calculate the probability of there being exactly two clonal variants as the probability that there are exactly two mutations that arise during the generation of the first mutant lineage and no clonal variants that arise thereafter, plus the probability that exactly one mutation arises during the generation of the first mutant lineage and exactly one clonal variant arising thereafter:

$$\begin{aligned}
P_{2,n=N} &= P_{1+,n=N} \times \left( \frac{\text{Poiss}(2, \mu)}{1 - \text{Poiss}(0, \mu)} \right) \times \left( \frac{P_{0,n=1}}{1 - P_{X,n=1}} \right) + \\
&= P_{1+,n=N} \times \left( \frac{\text{Poiss}(1, \mu)}{1 - \text{Poiss}(0, \mu)} \right) \times \left( \frac{P_{1,n=1}}{1 - P_{X,n=1}} \right)
\end{aligned}$$

Luckily, we can directly calculate all of these terms, including  $P_{1,n=1}$ , which is given by:

$$P_{1,n=1} = P_{1+,n=1} \times \left( \frac{\text{Poiss}(1, \mu)}{1 - \text{Poiss}(0, \mu)} \right) \times \left( \frac{P_{0,n=1}}{1 - P_{X,n=1}} \right)$$

Next, the probability of observing exactly  $k = 3$  clonal variants is given by the sum of the probability of 3 clonal variants arising during the generation of the first mutant lineage (and none thereafter), the probability of 2 clonal variants arising during the generation of the first mutant lineage (and 1 therefore), and the probability of 1 clonal variant arising during the generation of the first mutant lineage (and 2 thereafter). More generally, therefore, the probability of observing exactly  $k$  clonal variants is given by:

$$P_{k,n=N} = P_{1+,n=N} \sum_{i=1}^k \left( \frac{\text{Poiss}(i, \mu)}{1 - \text{Poiss}(0, \mu)} \right) \left( \frac{P_{k-i,n=1}}{1 - P_{X,n=1}} \right)$$

At this point, we now have  $P_{X,n=N}$  and  $P_{k,n=N}$ , for  $k \geq 0$ . Because we would not observe infections in recipients in the case of  $P_{X,n=N}$ , the final probability mass distribution for the number of clonal variants observed in a recipient is given by:

$$\rho_{k,n=N} = \frac{P_{k,n=N}}{1 - P_{X,n=N}}$$

for  $k \geq 0$  (Figure S1F).

Code for this inference approach (in both R and Matlab) is available from our GitHub site: <https://github.com/koellelab/nbclonal>. This site also includes an R package to calculate clonal variant probabilities.

***Rederivation of the Bozic et al. (2016) equation for the mean number of clonal variants***

Bozic et al. (2016) derived an equation for the expected number of clonal variants under a scenario of a population size starting with a single individual ( $N = 1$ ). In their work, the underlying model was a birth-death model with parameter  $\delta$  defined as the ratio of death rate to birth rate ( $d/b$ ) and parameter  $u$  defined as the probability of a mutation occurring during the production of an offspring. The equation they derived for the mean number of clonal variants is given by their equation (46):  $\delta u / (1 - \delta)$ .

Our underlying model is a branching process model, parameterized with a geometric offspring distribution. This distribution corresponds to the offspring distribution realized in a birth-death model. Our branching process model has parameter  $R_0$  defined as the ratio of birth rate to death rate (such that  $1/R_0$  is the ratio of death rate to birth rate,  $\delta$ ). Our model also has parameter  $\mu$ , defined as the mean number of mutations that occur at birth, with the distribution of mutations occurring at birth being Poisson distributed. The probability that zero mutations occur during the production of an offspring is thus given as  $e^{-\mu}$ . When  $\mu$  is small, the probability that a (single) mutation occurs during the production of an offspring is  $1 - e^{-\mu}$ , which is approximately  $\mu$ . As such, when  $\mu$  is small, it is approximately equal to Bozic et al.'s  $u$  parameter. Finally, to correspond with the assumption in (Bozic et al., 2016) of the population starting with a single individual, we set the initial viral population size  $N$  to 1.

With a small mutation rate  $\mu$ , the possible outcomes shown in Figure 1E consist primarily of  $S_\infty$ ,  $S_0$ , and  $S_1$ , and the probability that more than one clonal variant establishes within the  $S_1$  outcome is negligibly small. As such, the mean number of clonal variants is given by  $S_1$  conditional on infection, such that  $\bar{m}_{clonal} = S_1 / (1 - S_0)$ . This is equivalent to  $\bar{m}_{clonal} = (1 - S_\infty - S_0) / (1 - S_0)$ . As detailed above,  $S_0 = 1/R_0$  when  $N = 1$ . When  $\mu$  is small, we can

approximate  $S_\infty$  as  $1 - 1/(R_0 e^{-\mu}) = 1 - 1/(R_0(1 - \mu))$ . Substituting, the numerator becomes:  $(1 - S_\infty - S_0) = \mu/R_0 = \delta u$ , and the denominator becomes  $(1 - S_0) = 1 - 1/R_0 = 1 - \delta$ . As such, the expected number of clonal variants from our analytical expressions, parameterized with  $N = 1$ , agree with equation (46) provided in Bozic et al. (2016).

### ***Calculation of the mean transmission bottleneck size $\bar{N}_b$***

Then mean bottleneck size is given by:

$$\bar{N}_b = \sum_{b=1}^{\infty} b p_b(\lambda, R_0)$$

where  $p_b(\lambda, R_0)$  denotes the probability that the bottleneck size is  $b$  in a successful infection. In turn,  $p_b(\lambda, R_0)$  is given by:

$$p_b(\lambda, R_0) = \sum_{N=b}^{\infty} \frac{p_N(\lambda) \Pr(b, N, 1 - 1/R_0)}{1 - \Pr(0, N, 1 - 1/R_0)}$$

where  $\Pr(b, N, 1 - 1/R_0)$  is given by the binomial probability that exactly  $b$  out of the  $N$  initial viral particles successfully leave genetic lineages in the recipient host. This binomial probability is calculated using a success probability of  $1 - 1/R_0$  for each initial viral particle.

### ***Quantification of the number of clonal variants for the influenza A virus data set***

We applied our inference approach to a previously published IAV transmission pair data set from Michigan, USA (McCrone et al., 2018). The raw sequencing data have previously been made available by the authors (SRA BioProject: PRJNA412631). Individuals in the same household were considered transmission pairs if they displayed symptoms within 7 days of one another, were both positive for the same IAV subtype, and were infected with viruses that were genetically more similar to one another than 95% of epidemiologically unlinked pairs based on

the L1-norm. Transmission pairs with multiple putative donors for a single recipient were discarded. Further, pairs in which both individuals had symptom onset on the same day were discarded unless those were the first two positive individuals in their household. In these cases ( $N = 6$ ), both possible orderings of donor and recipient were evaluated. In total, our analysis included 46 unique transmission pairs and 52 possible orderings of donor-recipient transmissions.

Table S1 provides a list of the clonal variants identified in these transmission pairs and the frequencies that these clonal variants were observed at prior to the variant-calling threshold being applied. We used the datafile no cut trans freq.csv from McCrone et al. (2018)'s GitHub to calculate the number of clonal variants provided in this supplemental table.

### ***Quantification of the number of clonal variants for the SARS-CoV-2 data set***

We applied our inference approach to a previously published SARS-CoV-2 transmission pair data set from Austria (Popa et al., 2020). The raw sequencing data have previously been made available by the authors (SRA BioProject: PRJEB39849). To establish transmission pairs, the authors combined information on intrafamily cases with information on epidemiological transmission chains. Additional telephone investigations were used to validate inferred transmission pairs. The data set consisted of 39 transmission pairs as reported in Data File S4 from (Popa et al., 2020). Sequencing reads were downloaded from the SRA and variants were called relative to Wuhan/Hu-1 (NC 045512.2) as described in (Martin and Koelle, 2021). Table S2 provides a list of the clonal variants identified in these 39 transmission pairs and the frequencies that these clonal variants were observed at prior to the variant-calling threshold being applied. (Note that we have previously analyzed this data set using a 6% variant-calling threshold (Martin and Koelle, 2021). The reason we used this high threshold previously was to

remove spurious low frequency variants that were shared across many of the samples and therefore inflated transmission bottleneck size estimates based on shared genetic variation. Here, we use the variant-calling threshold to identify the sites that are monomorphic in both the donor and the recipient and therefore might be sites that harbor clonal variants in the recipient. As such, a lower variant-calling threshold yields a more conservative estimate on the number of clonal variants observed. In contrast, a higher variant-calling threshold yields a more conservative estimate of shared genetic variation.)

***Probability of a donor iSNV transmitting and fixing in a recipient***

We can calculate the probability that an iSNV that is observed at low frequency in the donor transmits and fixes in the recipient. This probability depends on the frequency of the iSNV in the donor ( $q$ ), the initial number of viral particles  $N$  and the within-host basic reproduction number  $R_0$ . The probability is given by:

$$\frac{\sum_{k=1}^N [\text{Binom}(k, N, q)(1/R_0)^{N-k}(1 - \text{Binom}(0, k, 1 - 1/R_0))]}{1 - P_X}$$

Figure S10 shows this probability over a range of  $N$  for IAV ( $R_0 = 11.1$ ) and for SARS-CoV-2 ( $R_0 = 7.4$ ). In both cases, it is clear that the probability that a low-frequency iSNV transmits and fixes is higher at lower  $N$ . This indicates that, if present, these iSNVs (which have the potential to be misidentified as clonal variants) are themselves evidence of small transmission bottleneck sizes. Note that the probability expression above assumes random sampling of viral particles from the donor.



## Supplemental Tables

Clonal variant	Transmission pair	Donor frequency (%)	Recipient frequency (%)	Used in 0.5% analysis?	Used in 3.0% analysis?	Used in 7.0% analysis?
<b>C193T</b>	321372->320645	2.3%	100%	N	Y	Y
<b>C263A</b>	321372->320645	0%	100%	Y	Y	Y
<b>A699G</b>	321372->320645	0%	100%	Y	Y	Y
<b>C1641T</b>	UM41510->UM40095	0%	100%	Y	Y	Y
<b>T1641C</b>	UM40093->UM41510	0%	100%	Y	Y	Y
<b>A543G</b>	UM41554->UM41553	0%	100%	Y	Y	Y
<b>C218T</b>	UM41554->UM41553	0%	100%	Y	Y	Y
<b>A2041G</b>	UM41554->UM41553	0%	100%	Y	Y	Y
<b>G543A</b>	UM40449->UM41554	0%	100%	Y	Y	Y
<b>T218C</b>	UM40449->UM41554	0%	100%	Y	Y	Y
<b>C1569T</b>	50319->50316	0%	100%	Y	Y	Y
<b>T1650G</b>	50319->50316	0%	99.9%	Y	Y	Y
<b>T487C</b>	50319->50316	0%	99.9%	Y	Y	Y
<b>A310G</b>	50468->50466	0%	100%	Y	Y	Y
<b>A1424G</b>	50553->50552	0%	99.1%	N	Y	Y
<b>A1701G</b>	50618->50619	3.4%	96%	N	N	Y
<b>G57A</b>	51138->51137	0%	100%	Y	Y	Y
<b>G517T</b>	51220->51216	6.1%	100%	N	N	Y
<b>C618T</b>	51220->51216	0%	99.9%	Y	Y	Y
<b>A1429G</b>	51220->51216	0%	99.8%	Y	Y	Y

**Table S1. Table of IAV clonal variants identified in the set of transmission pairs from McCrone et al. (2018).** For each clonal variant, the transmission pair in which it was identified is provided as are the frequencies of the variant in the donor and in the recipient.

Clonal variant	Transmission pair	Donor frequency (%)	Recipient frequency (%)	Used in 0.5% analysis?	Used in 3.0% analysis?	Used in 7.0% analysis?
C2509T	CoV_273->CoV_271	0%	96.7%	N	N	Y
G9526T	CoV_180->CoV_197	0%	96.6%	N	N	Y
C19255T	CoV_1062->CoV_218	0%	98.9%	N	Y	Y
C20457T	CoV_1057->CoV_177	3.6%	99.5%	N	N	Y
C20457T	CoV_1057->CoV_1058	3.6%	99.7%	N	N	Y
C20457T	CoV_1057->CoV_187	3.6%	99.6%	N	N	Y
T20458C	CoV_187->CoV_1068	0%	98.6%	N	Y	Y
G24102C	CoV_150->CoV_162	0.7%	99.9%	N	Y	Y
C26894T	CoV_162->CoV_161	0%	99.6%	Y	Y	Y

**Table S2. Table of SARS-CoV-2 clonal variants identified in the set of transmission pairs from Popa et al. (2020).** For each clonal variant, the transmission pair in which it was identified is provided as are the frequencies of the variant in the donor and in the recipient.

## Supplemental Figures

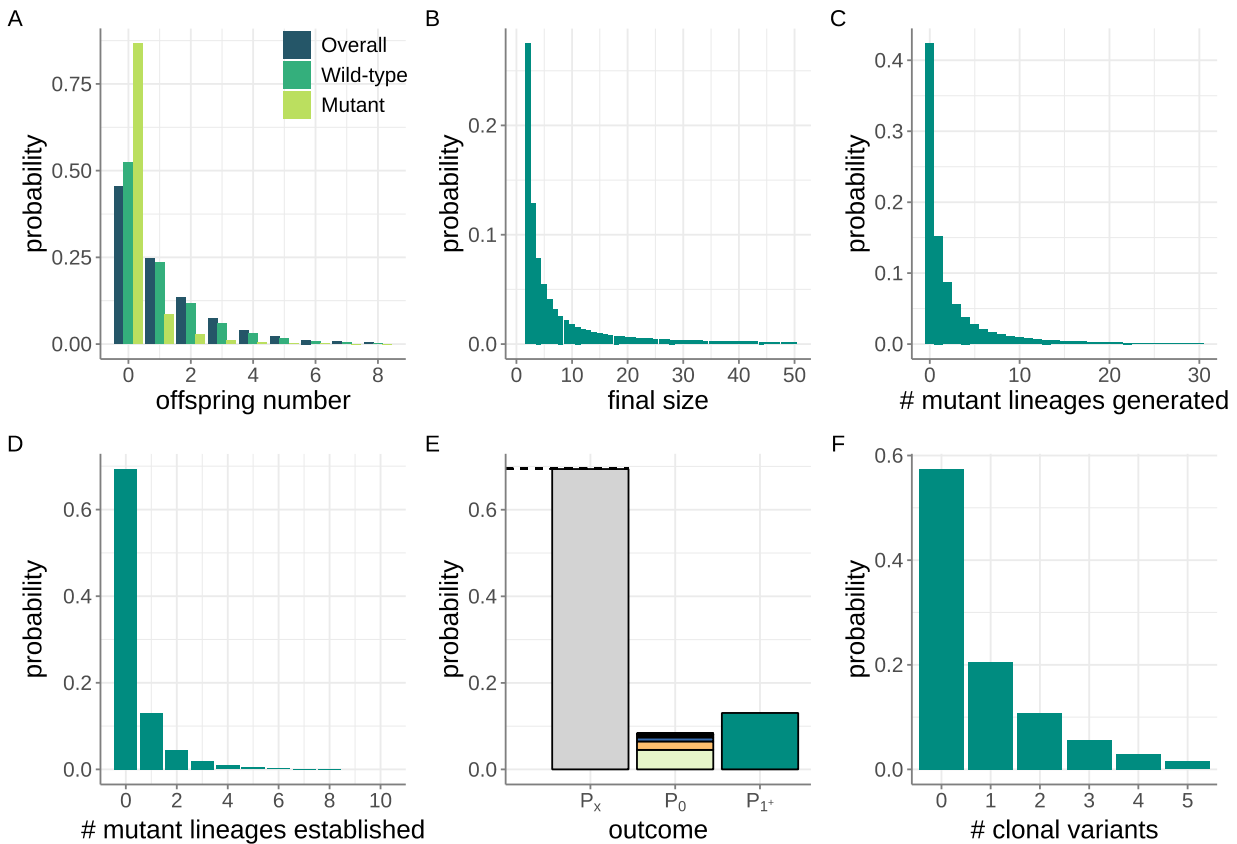


**Figure S1. Steps involved in the derivation of the probability mass function for the number of clonal variants.** (A) The overall offspring distribution, shown alongside the wild-type offspring distribution and the mutant offspring distribution. Here, the overall offspring distribution is a geometric distribution with mean  $R_0 = 1.2$  (such that  $p_{geom} = 0.4545$ ). The wild-type offspring distribution and the mutant offspring distribution are both negative binomial distribution with  $r_w$  and  $r_m$  calculated using a mutation rate of  $\mu = 0.2$ . (B) The final size distribution of wild-type particles, conditional on wild-type lineage extinction. Here, the initial number of viral particles  $N = 2$ . (C) The probability mass function for the number of mutant lineages generated by the wild-type viral population, conditional on wild-type lineage extinction. (D) The probability mass function for the number of mutant lineages that successfully establish, conditional on wild-type lineage extinction. (E) Calculated probabilities of the overall viral population going extinct ( $P_X$ , as calculated by  $S_0$ ), of the viral population establishing with zero clonal variants ( $P_0$ ), and of the viral population establishing with one or more clonal variants ( $P_{1+}$ ). Dashed black line shows the analytical calculation of  $P_X$  via the expression given by equation (3), indicating agreement with the calculated value of  $S_0$ . (F) Probability mass function for the number of clonal variants that establish in a recipient who becomes successfully infected.

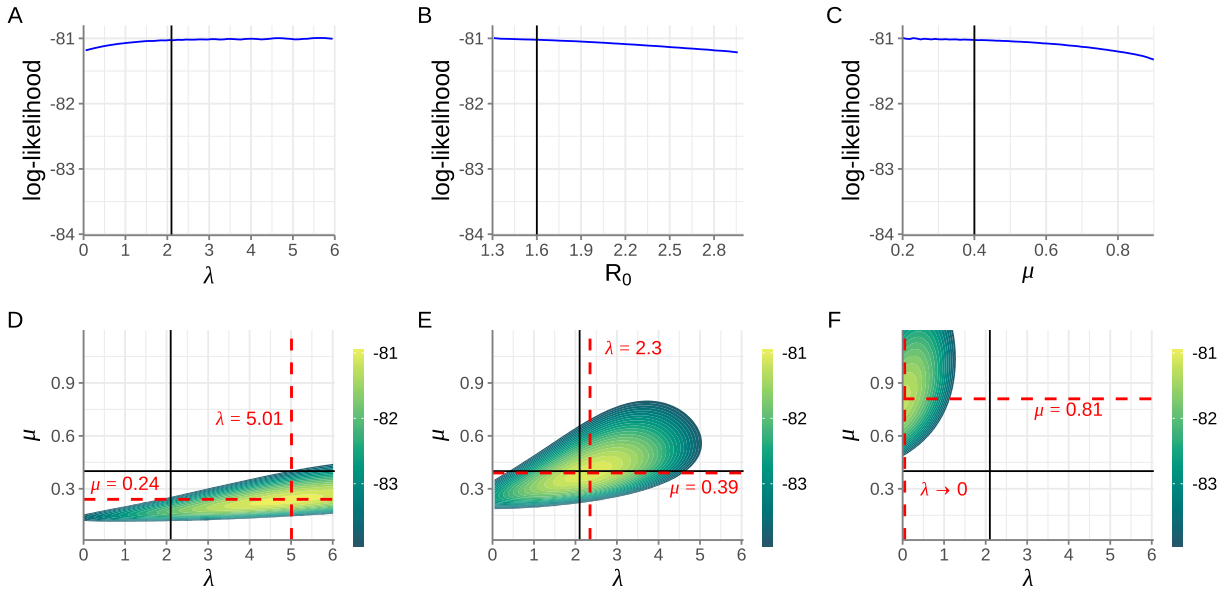


**Figure S2. Attempt at joint estimation of  $\lambda$ ,  $R_0$ , and  $\mu$ .** (A) Profile likelihood plot, showing the log(probability) of observing the mock data set across a range of  $\lambda$  values. (B) Profile likelihood plot, showing the log(probability) of observing the mock data set across a range of  $R_0$  values. (C) Profile likelihood plot, showing the log(probability) of observing the mock data set across a range of  $\mu$  values. In A-C, black vertical lines show the true parameter values used in the generation of the mock data set. (D) Log-likelihood plot, showing the log(probability) of observing the mock data set given parameters  $\lambda$  and  $\mu$ . Here,  $R_0$  was (erroneously) set to 1.3. (E) Log-likelihood plot, showing the log(probability) of observing the mock data set given parameters  $\lambda$  and  $\mu$ . Here,  $R_0$  was set to its true value of 1.6. (F) Log-likelihood plot, showing the log(probability) of observing the mock data set given parameters  $\lambda$  and  $\mu$ . Here,  $R_0$  was (erroneously) set to 3.0. In D-F, black lines show the true values of  $\lambda$  and  $\mu$  and red dashed lines show the maximum likelihood estimates of  $\lambda$  and  $\mu$ .

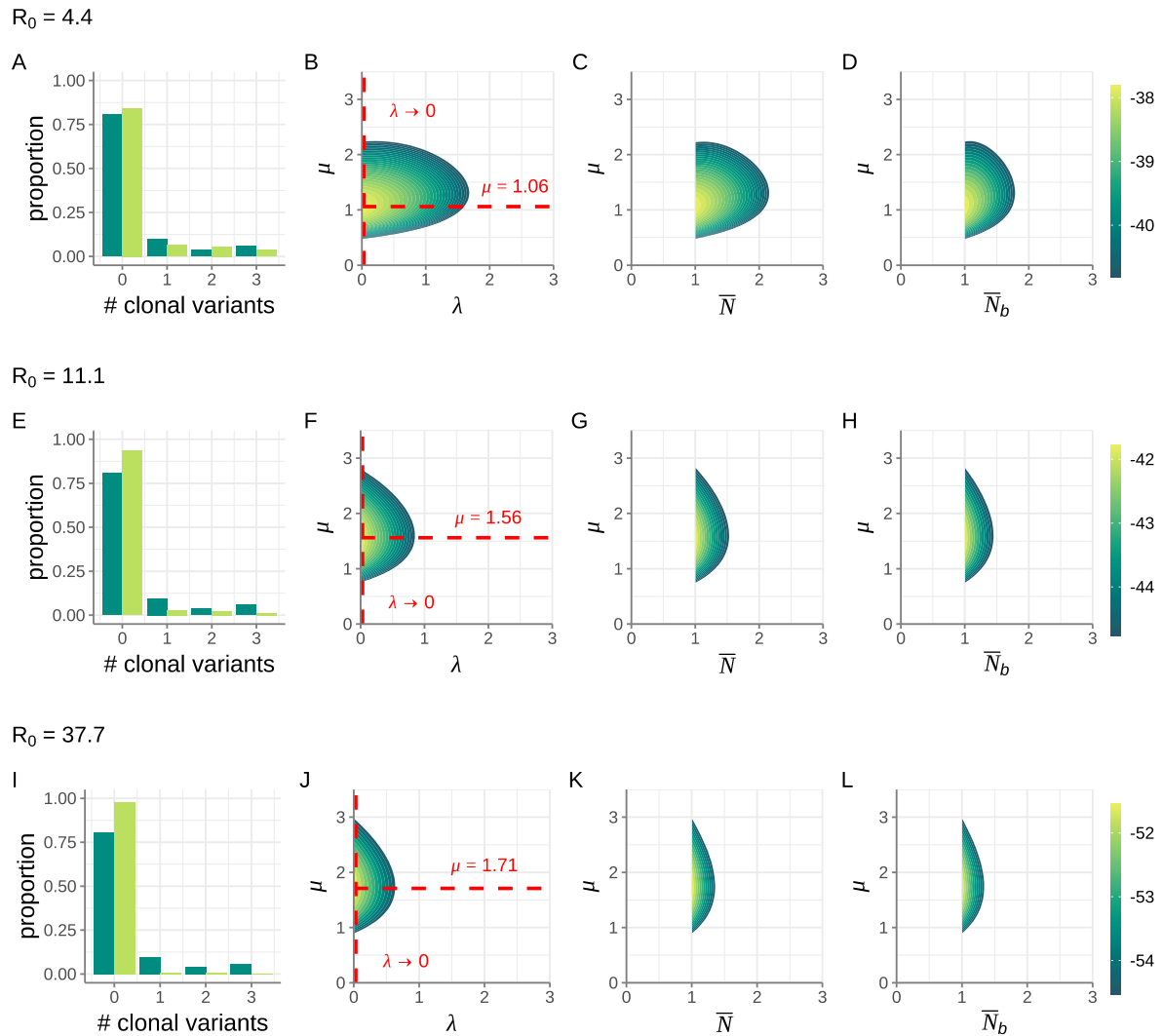


**Figure S3. Sensitivity analysis of IAV results across different assumptions of within-host  $R_0$ .** Results are shown in three rows, with the first row showing results with an assumed  $R_0$  value of 4.4, the second row showing results with an assumed  $R_0$  value of 11.1, and the third row showing results with an assumed  $R_0$  value of 37.7. For each  $R_0$  value considered, we plot four panels, analogous to those shown in the top row of Figure 4.

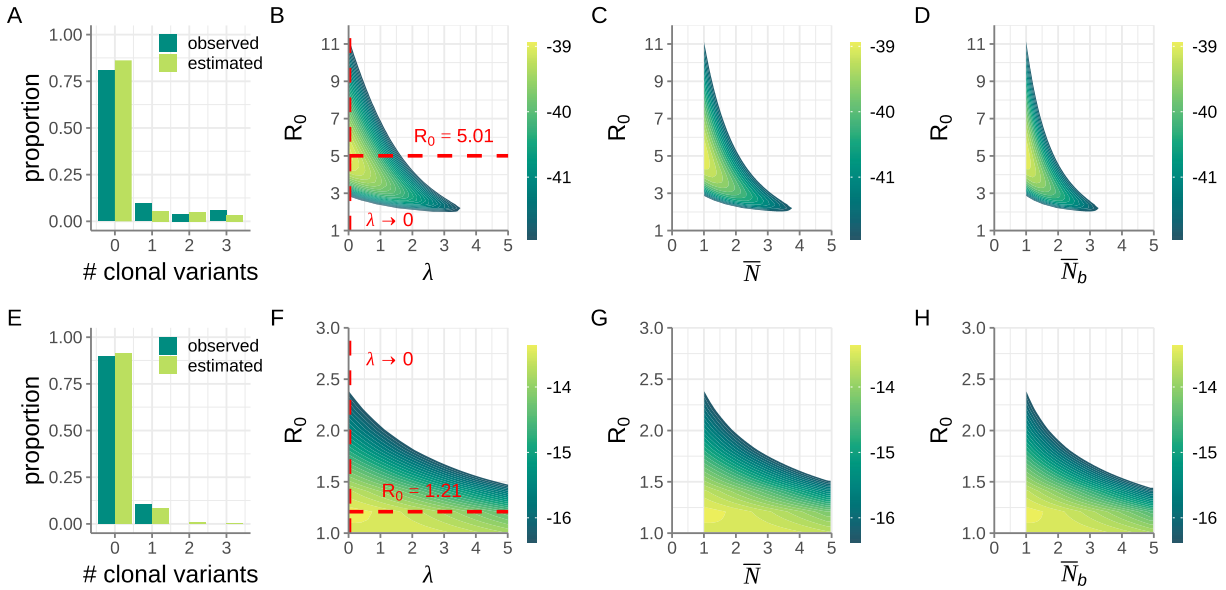


**Figure S4. Application of our inference method to influenza A virus (top row) and SARS-CoV-2 (bottom row) transmission pairs.** Here, we estimate  $\lambda$  and the within-host  $R_0$ , while setting the mutation rate  $\mu$  to estimates from the literature. **(A)** Distribution of the number of clonal variants observed across the 52 identified IAV transmission pairs (dark green bars). The expected distribution under the maximum likelihood estimates of  $\lambda$  and  $R_0$  (light green bars) is shown alongside the empirical distribution. **(B)** Log-likelihood plot, showing the log(probability) of observing the IAV data set across a range of  $\lambda$  and within-host  $R_0$  values. Dashed red lines show the maximum likelihood values for  $\lambda$  and  $R_0$ . **(C)** Log-likelihood plot, as in panel B, with the results plotted as a function of  $\bar{N}$  and  $R_0$  instead of  $\lambda$  and  $R_0$ . **(D)** Log-likelihood plot, as in panel B, with the results plotted as a function of  $\bar{N}_b$  and  $R_0$  instead of  $\lambda$  and  $R_0$ . **(E)** Distribution of the number of clonal variants observed across the 39 identified SARS-CoV-2 transmission pairs (dark green bars). The expected distribution under the maximum likelihood estimates of  $\lambda$  and within-host  $R_0$  (light green bars) is shown alongside the empirical distribution. **(F)** Log-likelihood plot, showing the log(probability) of observing the SARS-CoV-2 dataset across a range of  $\lambda$  and  $R_0$  values. **(G)** Log-likelihood plot, as in panel F, with the results plotted as a function of  $\bar{N}$  and  $R_0$  instead of  $\lambda$  and  $R_0$ . **(H)** Log-likelihood plot, as in panel F, with the results plotted as a function of  $\bar{N}_b$  and  $R_0$  instead of  $\lambda$  and  $R_0$ . In panels B-D and F-H, only the log-likelihood values that fall within the 95% confidence region are shown. For inference on the IAV data set, we set the mutation rate to  $\mu = 1.75$  mutations per genome per infection cycle, based on estimates from Pauly et al. (2017). For inference on the SARS-CoV-2 dataset, we set the mutation rate to  $\mu = 0.03$  mutations per genome per infection cycle, based on estimates from Amicone et al. (2022).

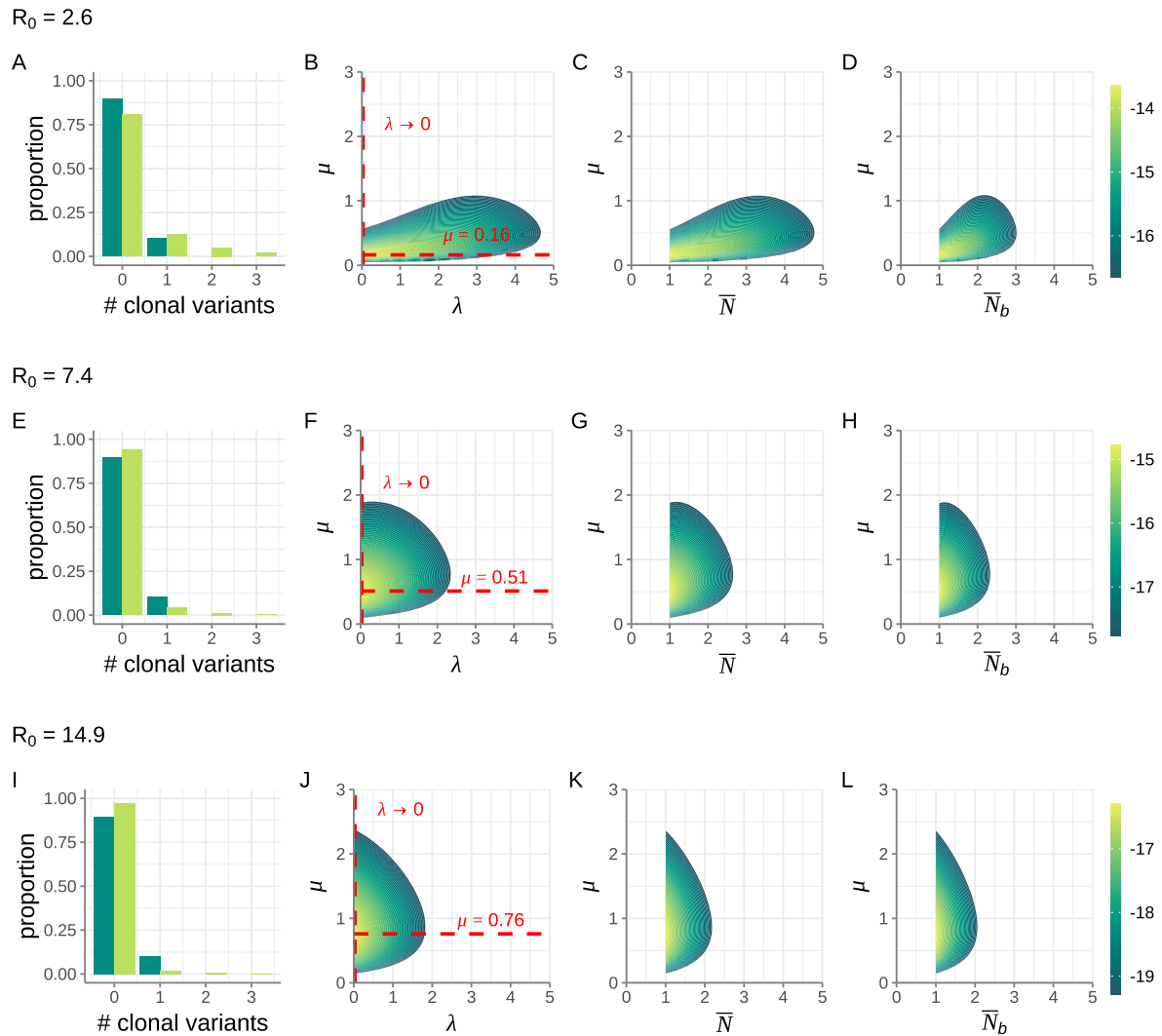


**Figure S5. Sensitivity analysis of SARS-CoV-2 results across different assumptions of within-host  $R_0$ .** Results are shown in three rows, with the first row showing results with an assumed  $R_0$  value of 2.6, the second row showing results with an assumed  $R_0$  value of 7.4, and the third row showing results with an assumed  $R_0$  value of 14.9. For each  $R_0$  value considered, we plot four panels, analogous to those shown in the bottom row of Figure 4.

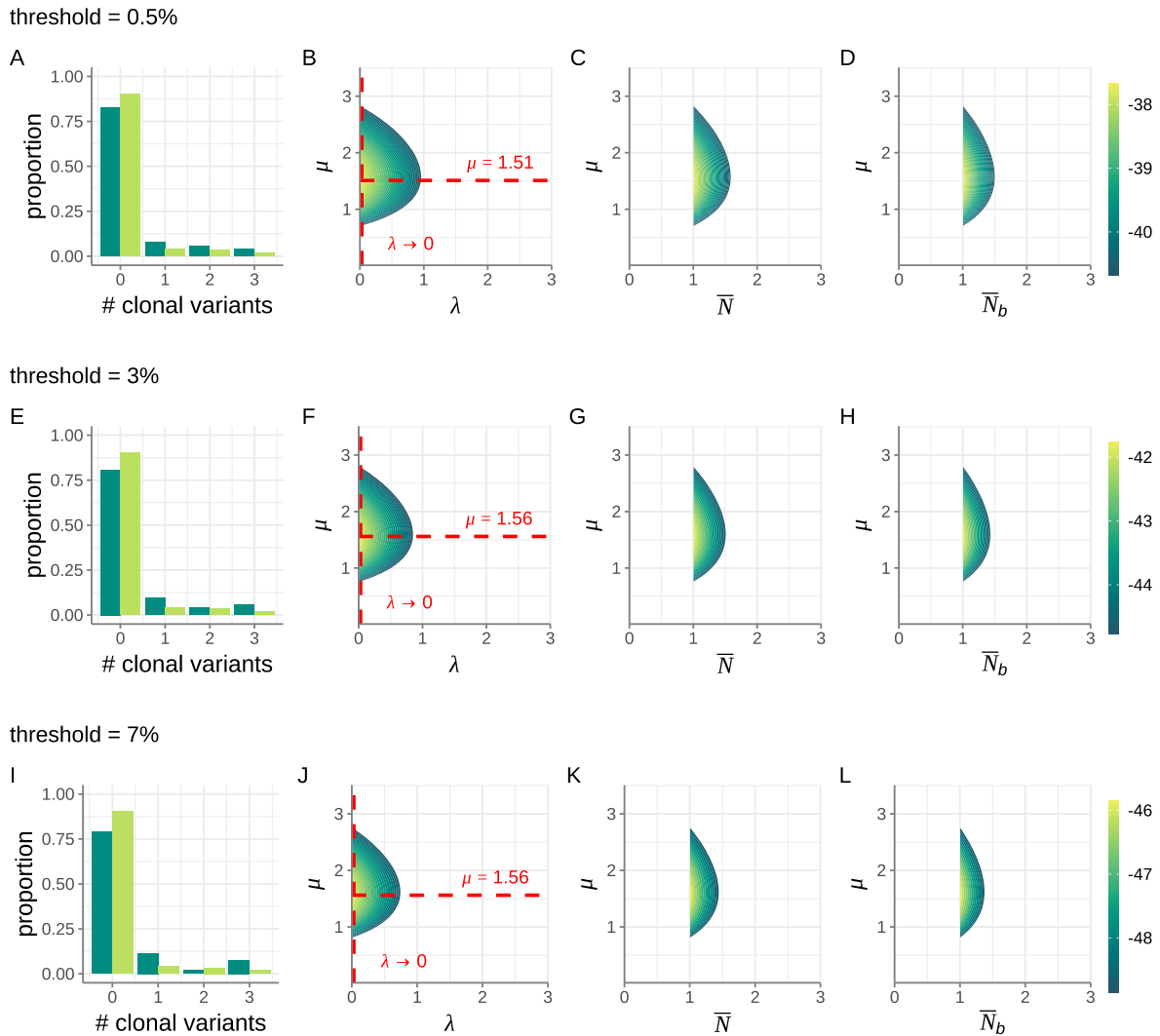


**Figure S6. Sensitivity analysis of IAV results across different variant-calling thresholds used. (A-D)** Inference results, as in Figures 4A-D, applying a variant calling threshold of 0.5%. **(E-H)** Inference results, as in Figures 4A-D, applying a variant calling threshold of 3%. (Identical to Figures 4A-D.) **(I-L)** Inference results, as in Figures 4A-D, applying a variant calling threshold of 7%. Notice that the distribution of the number of clonal variants observed across the transmission pairs can and does change with a change in the variant calling threshold applied.

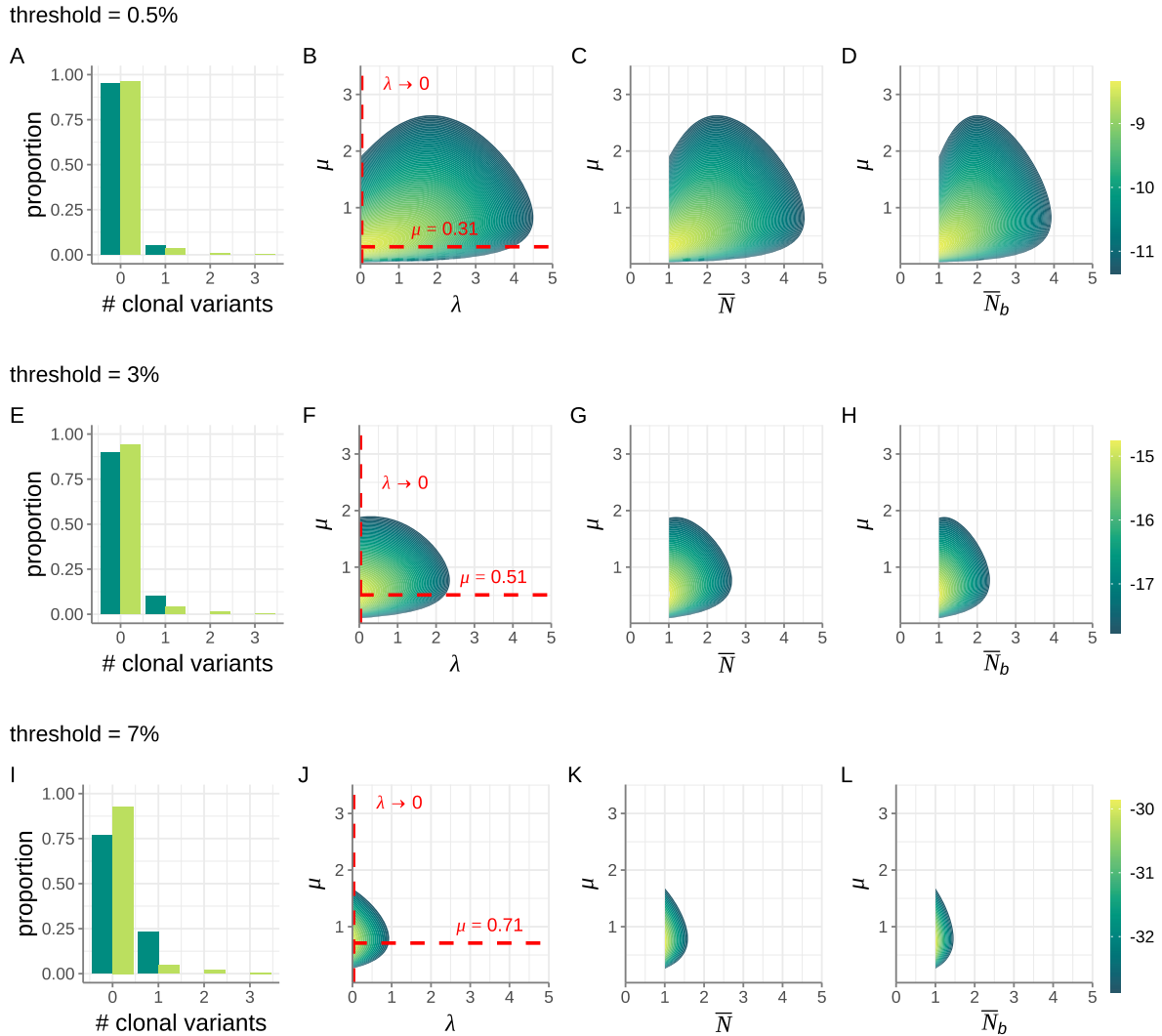


**Figure S7. Sensitivity analysis of SARS-CoV-2 results across different variant-calling thresholds used.** (A-D) Inference results, as in Figures 4E-H, applying a variant calling threshold of 0.5%. (E-H) Inference results, as in Figures 4E-H, applying a variant calling threshold of 3%. (Identical to Figures 4E-H.) (I-L) Inference results, as in Figures 4E-H, applying a variant calling threshold of 7%. Notice that the distribution of the number of clonal variants observed across the transmission pairs can and does change with a change in the variant calling threshold applied.



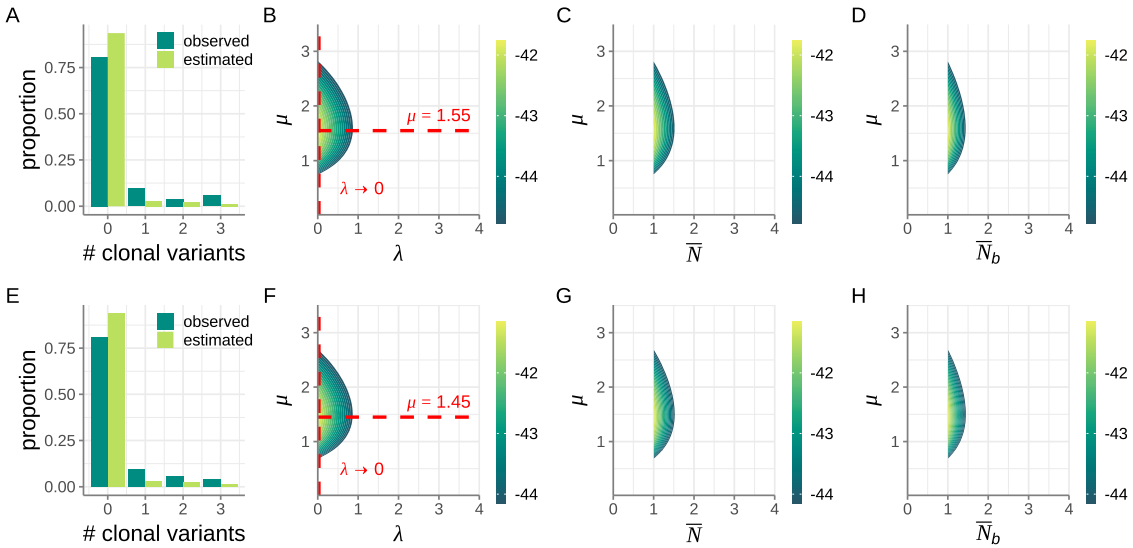


**Figure S8. Sensitivity analysis of IAV results when removing the potentially spurious clonal variant that is present in the donor at a frequency of 2.3%.** Top row reproduces the results shown in Figure 4 A-D. Bottom row shows inference results when this potentially spurious clonal variant was removed from the data set. Removal of this clonal variant resulted in a transmission pair previously classified as harboring three clonal variants being reclassified as harboring two clonal variants.

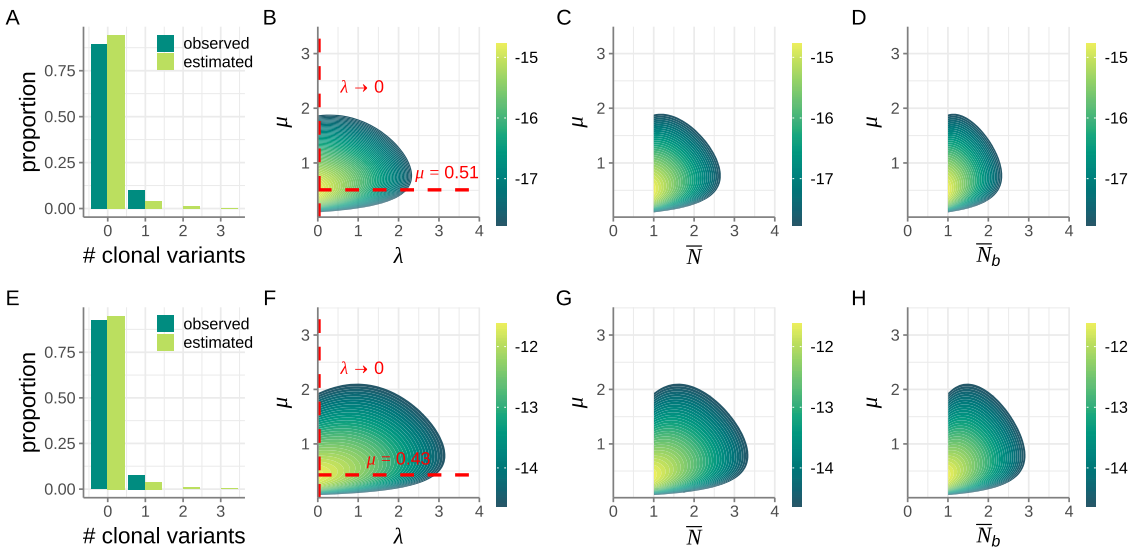


**Figure S9. Sensitivity analysis of SARS-CoV-2 results when removing the potentially spurious clonal variant that is present in the donor at a frequency of 0.7%.** Top row reproduces the results shown in Figure 4 E-H. Bottom row shows inference results when this potentially spurious clonal variant was removed from the data set. Removal of this clonal variant resulted in a transmission pair previously classified as harboring one clonal variant being reclassified as harboring no clonal variants.

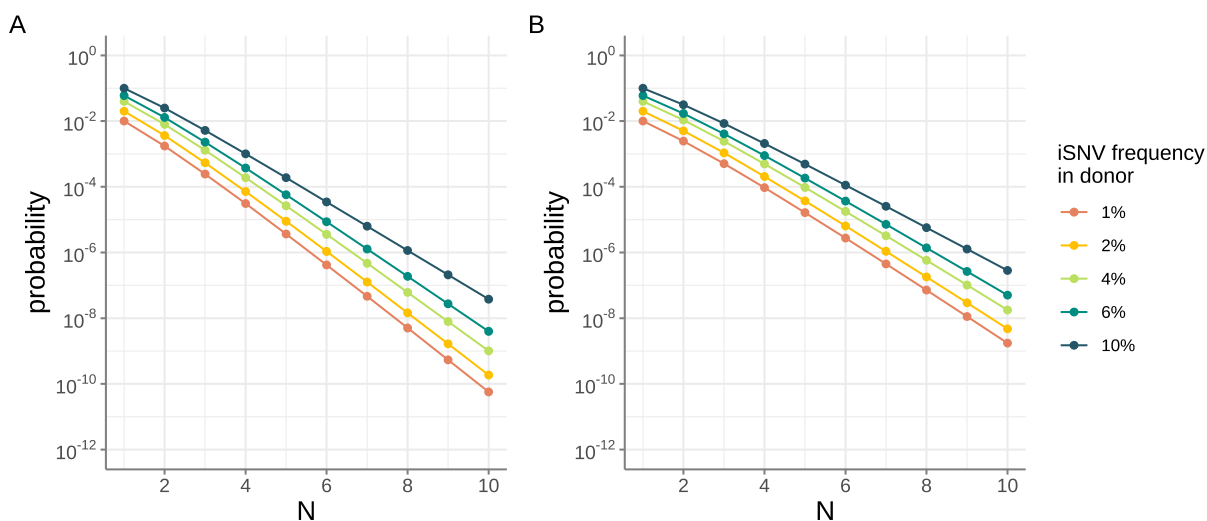


**Figure S10. Probability that a donor-derived iSNV transmits to the recipient and fixes, as a function of the initial number of viral particles that start off the infection in the donor. (A)**

Probabilities that an IAV iSNV present in a donor at 1%, 2%, 4%, 6%, and 10% transmits to the recipient and fixes. **(B)** Probabilities that a SARS-CoV-2 iSNV present in a donor at 1%, 2%, 4%, 6%, and 10% transmits to the recipient and fixes. In (A), the within-host  $R_0$  is set to 11.1. In (B), the within-host  $R_0$  is set to 7.4.

## References

Abel S, zur Wiesch PA, Davis BM, Waldor MK. Analysis of bottlenecks in experimental models of infection. *PLoS Pathog.* 2015;11(6):e1004823.

<https://doi.org/10.1371/journal.ppat.1004823>.

Amato KA, Haddock LA, Braun KM, Meliopoulos V, Livingston B, Honce R, Schaack GA, Boehm E, Higgins CA, Barry GL, et al. Influenza A virus undergoes compartmentalized replication in vivo dominated by stochastic bottlenecks. *Nat Commun.* 2022;13(1):3416.

<https://doi.org/10.1038/s41467-022-31147-0>.

Amicone M, Borges V, Alves MJ, Isidro J, Z'e-Z'e L, Duarte S, Vieira L, Guiomar R, Gomes JP, Gordo I. Mutation rate of SARS-CoV-2 and emergence of mutators during experimental

evolution. *Evol Med Public Health*. 2022;10(1):142–155.

<https://doi.org/10.1093/emph/eoac010>.

Baccam P, Beauchemin C, Macken CA, Hayden FG, Perelson AS. Kinetics of influenza A virus infection in humans. *J Virol*. 2006;80(15):7590–7599. <https://doi.org/10.1128/JVI.01623-05>.

Bendall EE, Callear AP, Getz A, Goforth K, Edwards D, Monto AS, Martin ET, Lauring AS. Rapid transmission and tight bottlenecks constrain the evolution of highly transmissible SARS-CoV-2 variants. *Nat Commun*. 2023;14(1):272. <https://doi.org/10.1038/s41467-023-36001-5>.

Betancourt M, Fereres A, Fraile A, García-Arenal F. Estimation of the effective number of founders that initiate an infection after aphid transmission of a multipartite plant virus. *J Virol*. 2008;82(24):12416–12421. <https://doi.org/10.1128/JVI.01542-08>.

Blumberg S, Lloyd-Smith JO. Comparing methods for estimating  $r_0$  from the size distribution of subcritical transmission chains. *Epidemics*. 2013a;5(3): 131–145.

Blumberg S, Lloyd-Smith JO. Inference of  $r_0$  and transmission heterogeneity from the size distribution of stuttering chains. *PLoS Comput Biol*. 2013b;9(5): e1002993.

Bozic I, Gerold JM, Nowak MA. Quantifying clonal and subclonal passenger mutations in cancer evolution. *PLoS Comput Biol*. 2016;12(2):e1004731. <https://doi.org/10.1371/journal.pcbi.1004731>.

Braun KM, Moreno GK, Halfmann PJ, Hodcroft EB, Baker DA, Boehm EC, Weiler AM, Haj AK, Hatta M, Chiba S, et al. Transmission of SARS-CoV-2 in domestic cats imposes a narrow bottleneck. *PLoS Pathog*. 2021a;17(2):e1009373. <https://doi.org/10.1371/journal.ppat.1009373>.

- Braun KM, Moreno GK, Wagner C, Accola MA, Rehrauer WM, Baker DA, Koelle K, O'Connor DH, Bedford T, Friedrich TC, et al. Acute SARS-CoV-2 infections harbor limited within-host diversity and transmit via tight transmission bottlenecks. *PLoS Pathog.* 2021b;17(8):e1009849. <https://doi.org/10.1371/journal.ppat.1009849>.
- Campbell F, Strang C, Ferguson N, Cori A, Jombart T, Parrish C. When are pathogen genome sequences informative of transmission events? *PLoS Pathog.* 2018;14(2):e1006885. <https://doi.org/10.1371/journal.ppat.1006885>.
- Duault H, Durang B, Canini L. Methods combining genomic and epidemiological data in the reconstruction of transmission trees: a systematic review. *Pathogens.* 2022;11(2):252. <https://doi.org/10.3390/pathogens11020252>.
- Emmett KJ, Lee A, Khiabani H, Rabadan R. High-resolution genomic surveillance of 2014 ebolavirus using shared subclonal variants. *PLoS Curr.* 2015:7.
- Geoghegan JL, Senior AM, Holmes EC. Pathogen population bottlenecks and adaptive landscapes: overcoming the barriers to disease emergence. *Proc Royal Soc Ser B.* 2016;283(1837):20160727.
- Ghafari M, Lumby CK, Weissman D, Illingworth CJR. Inferring transmission bottleneck size from viral sequence data using a novel haplotype reconstruction method. *J Virol.* 2020;94(13):e00014–e00020. <https://doi.org/10.1128/JVI.00014-20>.
- Gutiérrez S, Michalakis Y, Blanc S. Virus population bottlenecks during within-host progression and host-to-host transmission. *Curr Opin Virol.* 2012;2(5):546–555. <https://doi.org/10.1016/j.coviro.2012.08.001>.

- Hall MD, Woolhouse ME, Rambaut A. Using genomics data to reconstruct transmission trees during disease outbreaks. *Rev Sci Techens*. 2016;35(1):287–296.  
<https://doi.org/10.20506/rst.issue.35.1.2412>.
- Ke R, Zitzmann C, Ho DD, Ribeiro RM, Perelson AS. In vivo kinetics of SARS-CoV-2 infection and its relationship with a person's infectiousness. *Proc Natl Acad Sci U S A*. 2021;118(49):e2111477118. <https://doi.org/10.1073/pnas.2111477118>.
- Keele BF, Giorgi EE, Salazar-Gonzalez JF, Decker JM, Pham KT, Salazar MG, Sun C, Grayson T, Wang S, Li H, et al. Identification and characterization of transmitted and early founder virus envelopes in primary HIV-1 infection. *Proc Natl Acad Sci U S A*. 2008;105(21):7552–7557. <https://doi.org/10.1073/pnas.0802203105>.
- Li B, Deng A, Li K, Hu Y, Li Z, Shi Y, Xiong Q, Liu Z, Guo Q, Zou L, et al. Viral infection and transmission in a large, well-traced outbreak caused by the SARS-CoV-2 delta variant. *Nat Commun*. 2022;13(1):460. <https://doi.org/10.1038/s41467-022-28089-y>.
- Lloyd-Smith JO, Schreiber SJ, Kopp PE, Getz WM. Superspreading and the effect of individual variation on disease emergence. *Nature*. 2005;438(7066): 355–359.
- Lythgoe KA, Hall M, Ferretti L, de Cesare M, MacIntyre-Cockett G, Trebes A, Andersson M, Otecko N, Wise E, Moore N, et al. SARS-CoV-2 within-host diversity and transmission. *Science*. 2021;372(6539):eabg0821. <https://doi.org/10.1126/science.abg0821>.
- Martin MA, Koelle K. Comment on genomic epidemiology of superspreading events in Austria reveals mutational dynamics and transmission properties of SARS-CoV-2. *Sci Transl Med*. 2021;13(617):eabh1803. <https://doi.org/10.1126/scitranslmed.abh1803>.
- McCrone JT, Luring AS. Genetic bottlenecks in intraspecies virus transmission. *Curr Opin Virol*. 2018;28:20–25. <https://doi.org/10.1016/j.coviro.2017.10.008>.

- McCrone JT, Woods RJ, Martin ET, Malosh RE, Monto AS, Lauring AS. Stochastic processes constrain the within and between host evolution of influenza virus. *eLife*. 2018;7:e35962. <https://doi.org/10.7554/eLife.35962>.
- Moury B, Fabre F, Senoussi R. Estimation of the number of virus particles transmitted by an insect vector. *Proc Natl Acad Sci U S A*. 2007;104(45):17891–17896. <https://doi.org/10.1073/pnas.0702739104>.
- Nicholson MD, Endler L, Popa A, Genger JW, Bock C, Michor F, Bergthaler A. Response to comment on genomic epidemiology of superspreading events in Austria reveals mutational dynamics and transmission properties of SARS-CoV-2. *Sci Transl Med*. 2021;13(617):eabj3222. <https://doi.org/10.1126/scitranslmed.abj3222>.
- Nishiura H, Yan P, Sleeman CK, Mode CJ. Estimating the transmission potential of supercritical processes based on the final size distribution of minor outbreaks. *Journal of Theoretical Biology*. 2012;294: 48–55.
- Pauly MD, Procaro MC, Lauring AS. A novel twelve class fluctuation test reveals higher than expected mutation rates for influenza A viruses. *eLife*. 2017;6:e26437. <https://doi.org/10.7554/eLife.26437>.
- Poon LLM, Song T, Rosenfeld R, Lin X, Rogers MB, Zhou B, Sebra R, Halpin RA, Guan Y, Twaddle A, et al. Quantifying influenza virus diversity and transmission in humans. *Nat Genet*. 2016;48(2):195–200. <https://doi.org/10.1038/ng.3479>.
- Popa A, Genger JW, Nicholson MD, Penz T, Schmid D, Aberle SW, Agerer B, Lercher A, Endler L, Colaço H, et al. Genomic epidemiology of superspreading events in Austria reveals mutational dynamics and transmission properties of SARS-CoV-2. *Sci Transl Med*. 2020;12(573):2555. <https://doi.org/10.1126/scitranslmed.abe2555>.

- Sacristán S, Díaz M, Fraile A, García-Arenal F. Contact transmission of tobacco mosaic virus: a quantitative analysis of parameters relevant for virus evolution. *J Virol*. 2011. <https://doi.org/10.1128/JVI.00057-11>.
- Sanjuán R. Collective infectious units in viruses. *Trends Microbiol*. 2017;25(5):402–412. <https://doi.org/10.1016/j.tim.2017.02.003>.
- Sobel Leonard A, McClain MT, Smith GJ, Wentworth DE, Halpin RA, Lin X, Ransier A, Stockwell TB, Das SR, Gilbert AS, et al. The effective rate of influenza reassortment is limited during human infection. *PLoS Pathog*. 2017a;13(2):e1006203. <https://doi.org/10.1371/journal.ppat.1006203>.
- Sobel Leonard A, Weissman DB, Greenbaum B, Ghedin E, Koelle K. Transmission bottleneck size estimation from pathogen deep-sequencing data, with an application to human influenza A virus. *J Virol*. 2017b;91(14):e00171-17. <https://doi.org/10.1128/JVI.00171-17>.
- Valesano AL, Fitzsimmons WJ, McCrone JT, Petrie JG, Monto AS, Martin ET, Lauring AS. Influenza B viruses exhibit lower within-host diversity than influenza A viruses in human hosts. *J Virol*. 2020;94(5):e01710-19. <https://doi.org/10.1128/JVI.01710-19>.
- Varble A, Albrecht RA, Backes S, Crumiller M, Bouvier NM, Sachs D, García-Sastre A, tenOever BR. Influenza A virus transmission bottlenecks are defined by infection route and recipient host. *Cell Host Microbe*. 2014;16(5):691–700. <https://doi.org/10.1016/j.chom.2014.09.020>.
- Visher E, Whitefield SE, McCrone JT, Fitzsimmons W, Lauring AS. The mutational robustness of influenza A virus. *PLoS Pathog*. 2016;12(8):e1005856. <https://doi.org/10.1371/journal.ppat.1005856>.

Wang D, Wang Y, Sun W, Zhang L, Ji J, Zhang Z, Cheng X, Li Y, Xiao F, Zhu A, et al.

Population bottlenecks and intra-host evolution during human-to-human transmission of SARS-CoV-2. *Nat Commun.* 2021;15(8):585358.

Zaraket H, Baranovich T, Kaplan BS, Carter R, Song M-S, Paulson JC, Rehg JE, Bahl J,

Crumpton JC, Seiler J, et al. Mammalian adaptation of influenza A (H7N9) virus is limited by a narrow genetic bottleneck. *Nat Commun.* 2015;6(1):6553.

<https://doi.org/10.1038/ncomms7553>.

Zwart MP, Elena SF. Matters of size: genetic bottlenecks in virus infection and their potential

impact on evolution. *Annu Rev Virol.* 2015;2(1):161–179.

<https://doi.org/10.1146/virology.2015.2.issue-1>.